An integrated carbon and oxygen isotope approach to reconstructing past environmental variability in the northeast Atlantic Ocean

David J. Reynolds[a,b,*], Ian R. Hall[a], Sophie M. Slater[a]

[a] *School of Earth and Ocean Science, Cardiff University, Park Place, Cardiff CF10 3AT, UK*
[b] *Laboratory of Tree Ring Research, University of Arizona, Tucson, AZ 85721, USA*

ABSTRACT

The combined influence of temperature and the isotopic composition of the seawater ($\delta^{18}O_w$) often precludes the use of oxygen isotope ($\delta^{18}O$) records, derived from marine carbonates, to reconstruct absolute seawater temperatures, without the application of an independent $\delta^{18}O_w$ proxy. Here we investigate the application of carbon isotope records ($\delta^{13}C_{shell}$), derived from the long-lived marine bivalve *Glycymeris glycymeris*, as a proxy for $\delta^{18}O_w$ variability. Our analyses indicate *G. glycymeris* $\delta^{13}C_{shell}$ data derived from growth increments > 20 years of age contain strong ontogenetic trends ($-0.013‰ \, yr^{-1}$, $R = 0.98$, $P < 0.001$, $N = 51$). These analyses demonstrate that, coupled with the ontogenetic trends, 54% of the variability in *G. glycymeris* $\delta^{13}C_{shell}$ records can be explained by a combination of the marine Suess effect and physical (salinity and riverine input) and biological processes (primary production). The application of these $\delta^{13}C_{shell}$ data in conjunction with co-registered $\delta^{18}O_{shell}$ and growth increment width series, each of which have been shown to be sensitive to seawater temperature and primary productivity respectively, can therefore provide new insights into past environmental variability and help constrain uncertainties on reconstructions of past seawater temperature variability.

1. Introduction

The widespread application of oxygen stable isotope ($\delta^{18}O$) records for reconstructing past oceanographic variability is largely due to the well characterised mechanisms that drive $\delta^{18}O$ variability in marine carbonates ($\delta^{18}O_{carb}$; temperature and the $\delta^{18}O$ composition of seawater [$\delta^{18}O_w$], which is closely related to salinity), and the broad spectrum of marine archives that provide long-term records of $\delta^{18}O$ variability (e.g. planktonic and benthic foraminifera, corals, otoliths and molluscs; Urey, 1948, Shackleton et al., 1984, Chappell and Shackleton, 1986, Fairbanks and Matthews, 1978, Chappell et al., 1996, Schöne et al., 2005, Wanamaker Jr. et al., 2011, Reynolds et al., 2016). Whilst $\delta^{18}O_{carb}$ records have proved invaluable in developing our understanding of past marine variability, the combined influence of both temperature and $\delta^{18}O_w$ on the $\delta^{18}O_{carb}$ variability typically precludes the reconstruction of absolute water temperature or $\delta^{18}O_w$ without using an independent proxy for $\delta^{18}O_w$ or seawater temperature respectively. To mitigate this issue $\delta^{18}O_{carb}$ records derived from foraminifera can be integrated with coupled (co-registered) magnesium/calcium (Mg/Ca) ratios (e.g. Elderfield and Ganssen, 2000). As the Mg/Ca ratios in some foraminifera faithfully reflect the ambient seawater temperature at the time of carbonate formation, the integration of Mg/

Ca and $\delta^{18}O$ analyses can facilitate the quantitative reconstruction of past seawater temperature and/or $\delta^{18}O_w$. However, such techniques have hitherto been shown to be ineffective in proxy records derived from the geochemical analysis of long-lived marine bivalves (sclerochronologies). While there are exceptions (e.g. *Pectin maximums* (Freitas et al., 2012), Mg/Ca records from the majority of marine bivalve species contain little, if any, coherence with seawater temperature (e.g. Lorens and Bender, 1980; Vander Putten et al., 2000; Lorrain et al., 2005; Freitas et al., 2005; Freitas et al., 2008; Wanamaker et al., 2008b). In the majority of marine bivalves a number of mechanisms have been demonstrated to drive Mg/Ca ratios including metabolic processes, ontogeny, the organic matrix of the shell, intra-shell variability and salinity (Freitas et al., 2012 and references there in). Given the lack of a stable coherence between molluscan Mg/Ca ratios and temperature alternative approaches have to be employed for detangling the influence of seawater temperature and $\delta^{18}O_w$ on $\delta^{18}O_{shell}$ records.

Several studies have previously suggested that molluscan $\delta^{13}C$ records ($\delta^{13}C_{shell}$) could be used as a potential proxy for $\delta^{18}O_w$/salinity (Gillikin et al., 2005; Gillikin et al., 2006). The application of $\delta^{13}C_{shell}$ records as a proxy for $\delta^{18}O_w$ would be advantageous as these data are generated simultaneously with the $\delta^{18}O_{shell}$ records and thus not require any additional analyses. However, $\delta^{13}C_{shell}$ variability has been

demonstrated to be a combined function of both internal biological processes and external processes (Tanaka et al., 1986; Klein et al., 1996; McConnaughey et al., 1997; Lorrain et al., 2004; Gillikin et al., 2005, 2006, 2007 – also reviewed in McConnaughey and Gillikin, 2008; Wanamaker et al., 2009, Schöne et al., 2011, Beirne et al., 2012; Reynolds et al., 2017a). External processes drive changes in the $\delta^{13}C$ composition of dissolved inorganic carbon ($\delta^{13}C_{DIC}$) in the ambient water through both physical (temperature, salinity and air-sea pCO_2 exchange) and biological (primary production) processes (Lynch-Stieglitz et al., 1995). On the other hand, internal biological processes either directly lead to the fractionation of the $\delta^{13}C_{DIC}$ or lead to a change in the proportion of environmental and respired carbon being incorporated into the shell matrix through time (McConnaughey and Gillikin, 2008; Beirne et al., 2012). In some marine bivalve species, these processes have been argued to vary with age and are therefore termed ontogenetic effects (Lorrain et al., 2004).

In recent years an increasing number of studies have sought to utilise the growth increment width series and $\delta^{18}O_{shell}$ records derived from the long-lived marine bivalve *Glycymeris glycymeris* to investigate past marine variability (e.g. Brocas et al., 2013; Reynolds et al., 2013; Royer et al., 2013; Featherstone et al., 2017; Reynolds et al., 2017b). However, hitherto the application of the corresponding *G. glycymeris* $\delta^{13}C_{shell}$ data has yet to be investigated. Utilising *G. glycymeris* $\delta^{13}C_{shell}$ data to study past carbon dynamics would be advantageous as *G. glycymeris* populate contrasting habitats (coarser grain size substrates; Hayward and Ryland, 1995) to that of other commonly used sclerochronological archives (e.g. *Arctica islandica*) and thus could provide unique perspectives on carbon cycle dynamics in a broader spectrum of environments across the North Atlantic continental shelf seas. However, due the potential of ontogenetic $\delta^{13}C_{shell}$ trends, it is necessary to develop a better understanding of the mechanisms and processes controlling $\delta^{13}C_{shell}$ variability in *G. glycymeris*.

In this study we aim to examine: i) whether *G. glycymeris* $\delta^{13}C_{shell}$ series contain significant ontogenetic trends; ii) whether it is possible to combine $\delta^{13}C_{shell}$ data from multiple *G. glycymeris* shells to construct $\delta^{13}C_{shell}$ datasets that can extend beyond the longevity of a single specimen; and 3) to what extent environmental variability (primary production, riverine input, seawater temperature and salinity) drive variability in *G. glycymeris* $\delta^{13}C_{shell}$ timeseries.

2. Material and methods

2.1. Sampling and study site

Live and fossil *G. glycymeris* and *A. islandica* shells were collected from the Tiree Passage, off the western coast of Scotland, by mechanical dredge, deployed by the *RV Prince Madog*, and scuba diving (Natural Environment Research Council [NERC] National Facility for Scientific Diving) between 2006 and 2014. The shells were collected from water depths between 25 and 55 m in the vicinity of Tiree Passage oceanographic mooring (56°37.75N, 6°24.00W, Fig. 1). For full details of the shell collection see Reynolds (2011), Reynolds et al. (2013) and Reynolds et al. (2017b).

Due to its locality on the northwest European shelf, variability in the Tiree Passage is dominated by tidal mixing and the northward advection of warm salty water that is entrained into the Sea of the Hebrides, principally from the European Slope Current (ESC) and the North Atlantic Current (NAC; Inall et al., 2009, Marsh et al., 2017) respectively. Variability in the ESC is tightly linked to the dynamics of the North Atlantic subpolar gyre (SPG) circulation and the Atlantic Meridional Overturning Circulation (AMOC), being driven both by wind driven Ekman transport and latitudinal, salinity driven, density gradients (Marsh et al., 2017).

Several observational records exist from the northwest Scottish coastal region including seawater temperature and salinity measurements in the Tiree Passage (Inall et al., 2009) and nearby Keppel Pier

(www.bodc.ac.uk/data/), primary production measured as part of the Continuous Plankton Recorder dataset (CPR; www.sahfos.ac.uk/) and river flow data from the river Ewe spanning the interval from 1971 to 2016 (https://nrfa.ceh.ac.uk/data). However, no direct measurements of the $\delta^{13}C_{DIC}$ are available from this region (Schöne et al., 2011). To mitigate this issue, we utilised $\delta^{13}C_{shell}$ data derived from annually resolved and crossdated *A. islandica* shells, that have been demonstrated to faithfully record seawater $\delta^{13}C_{DIC}$ (Beirne et al., 2012), collected from the Tiree Passage to evaluate if the *G. glycymeris* $\delta^{13}C_{shell}$ data are likely consistent with $\delta^{13}C_{DIC}$ variability in the Tiree Passage.

2.2. Sample preparation

Both the *A. islandica* and *G. glycymeris* shells were sectioned using standard sclerochronological procedures (Ramsay et al., 2000; Richardson, 2001). A rough 1–2 cm section of shell was cut using a diamond tipped blade rotary saw to remove the portion of shell containing the axis of maximum growth from the apex of the hinge through to the ventral margin. The shell section containing the axis of maximum growth was then embedded into MetPrep epoxy resin before a final cut was made adjacent to the axis of maximum growth using diamond tipped blades mounted on Buehler Isomet 4000 and Isomet 5000 saws. The final cut shell sections were then polished using carborundum paper using finer grades of grit (from grade 120–2000; equivalent of down to 3 μm grit size) and polished using a 3 μm diamond paste and neoprene polishing cloth.

Acetate peel replicas were constructed of the polished and etched (using 0.1M hydrochloric acid for 90 and 120 s for *G. glycymeris* and *A. islandica* respectively) shell surfaces to facilitate the identification and measurement of the growth increment widths. Digital photographs were taken of the acetate peel replicas using transmitted light microscopes and 3-megapixel digital cameras under between ×2 and ×10 magnification. Numerous systems were used to image the acetate peel replicas (e.g. Soft Imaging System digital camera and AnalySIS imaging software and Image Pro Premiere software), for more details see Reynolds et al. (2013). The widths of each growth increment in each shell were digitally measured using the Buehler Omnimet and Image Pro Premier software.

2.3. Sample dating

Carbonate samples obtained from *G. glycymeris* shells that lived during the "modern" interval (1800 CE to present) were dated utilising the Tiree Passage *G. glycymeris* growth increment width chronology (Reynolds et al., 2013). The shells contained in this chronology were crossdated and the ages validated by accelerator mass spectrometry (AMS) radiocarbon (^{14}C) dating (Reynolds et al., 2013). Shells that lived in the "pre-modern" era (i.e. pre-1800 CE) were dated by AMS ^{14}C dating using the Natural Environment Research Council AMS ^{14}C facility (East Kilbride, UK). A single carbonate sample was cut from the outer shell layer of the ventral margin of 21 dead collected *G. glycymeris* shells. The ^{14}C determinations were calibrated into calendar dates using OxCal online V4.3 (Ramsey, 2009) using the Marine 13 radiocarbon calibration curve (Reimer et al., 2013). A regional offset (ΔR) from the marine calibration curve of 26 ± 14 years was applied to the calibrated ^{14}C dates (Cage et al., 2006). The dates of the annual $\delta^{13}C_{shell}$ samples derived from the ^{14}C dated shells were based on assigning the most modern growth increment the calendar year associated with the centre point of the 95.4% probability distribution generated by the OxCal ^{14}C calibration and growth band counting relative to this increment. Whilst this method increases the potential for temporal uncertainties, the clear nature of the annually resolved *G. glycymeris* growth increments mitigates this issue. For similar methodology see (Wanamaker et al., 2011).

The dates of the $\delta^{13}C_{shell}$ samples derived from the live collected *A. islandica* shells were based on crossdating. The growth increment
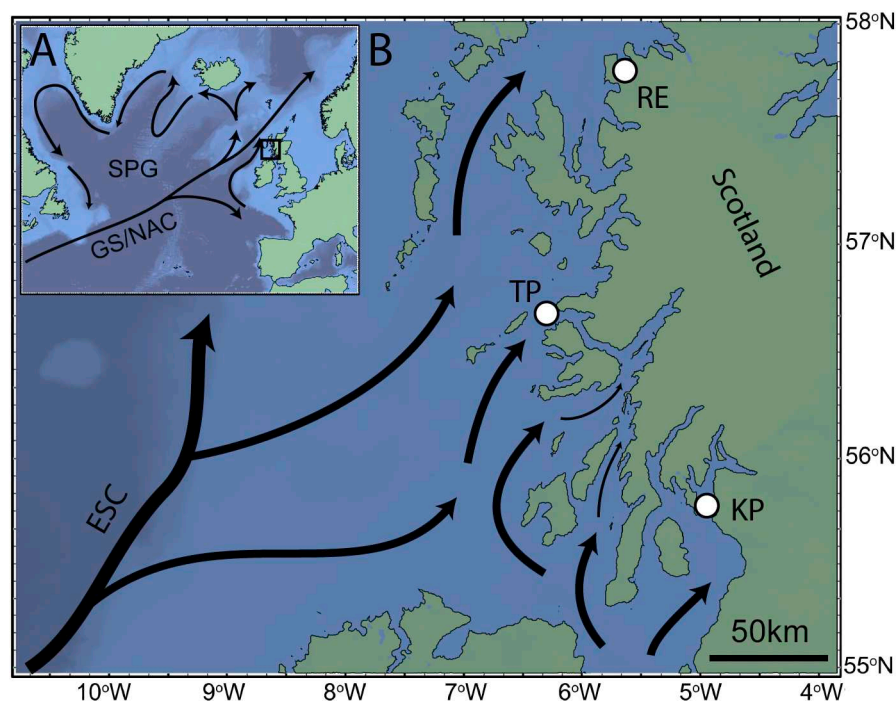
Fig. 1. Map showing the major currents of A) the North Atlantic and B) the continental shelf of north-western Scotland. Shell samples were collected from the Tiree Passage (TP). Oceanographic data were obtained from oceanographic instrumental moorings at both Keppel Pier (KP) and TP as well as river flow data from River Ewe (RE). The black arrows denote the general circulation pattern. SPG = subpolar gyre; GS/NAC = Gulf Stream/North Atlantic Current; ESC = European Slope Current.

widths of ten live collected *A. islandica* shells were crossdated using SHELLCORR, run in Matlab (Butler et al., 2010). The comparison of ten shells using crossdating allowed the generation of a suite of absolutely dated growth increments which then formed the temporal framework for the stable isotope analyses.

2.4. Isotope sampling

Aragonite powder samples, of between 10 µg and 400 µg, were drilled from the growth increments in the outer shell layer of a subset of shells contained in the Tiree Passage master sclerochronology, fossil *G. glycymeris* shells and three live-collected *A. islandica* shells. The same methodology was used for sampling each of these shells. Samples were drilled using a 300 µm tungsten carbide drill bit coupled to a Merchantek (New Wave) micromill system from the polished embedded shell sections. For an in-depth description of the micromilling methodology used for sampling see (Reynolds et al., 2017b) and Supplementary Fig. S1. In summary, for the annual resolution samples a single sample was drilled to a total depth of 1 mm from each growth increment. As the width of the growth increments varies this approach results in the generation of a variable amount of carbonate powder. In the cases where a large volume of powder was generated, due to the increments being wider, a subsample of the carbonate powder was analysed. We replicated the analyses of 107 subsamples from 13 individual shells to test if these larger samples were sufficiently homogenised. The standard deviation of these replicated samples was used to evaluate the homogenisation process. As part of the Reynolds et al. (2017a, 2017b) $\delta^{18}O_{shell}$ study isotope analyses were also conducted at sub-annual resolution, with multiple carbonate samples being drilled from within a single growth increment. To maximise the data available in this study we utilise the corresponding sub-annual resolution $\delta^{13}C_{shell}$ data. However, as the focus of this study is on inter-annual variability, the sub-annual data were down-scaled to annual resolution by calculating the arithmetic mean of the sub-annually resolved $\delta^{13}C_{shell}$ data within each individual growth increment sampled. As the sub-annual resolution sampled data were obtained from the same portion of shell as the annual data (Supplementary Fig. 1) the down-scaled data were treated as annually resolved in all further analyses. The effect of arithmetically averaging the sub-annual resolution $\delta^{13}C_{shell}$ data was evaluated by

performing linear regression analysis between the sampling resolution (the number of sub-annual resolution samples used to generate the annual $\delta^{13}C_{shell}$ value) and the corresponding annual mean value. These sub-annual derived values were then compared with annual resolution data, generated by drilling one sample per year, as part of the inter-shell $\delta^{13}C$ variability analyses (see results Section 3.3).

The $\delta^{13}C_{shell}$ composition of all samples was measured using a Thermo Mat 253 mass spectrometer coupled to a Kiel IV carbonate preparation device (Cardiff University). The shell samples were analysed alongside an internal standard made of Carrara marble (no less than six standards per 40 shell samples) and calibrated against international standard NBS-19, expressed relative to the Vienna Pee Dee Belemnite (VPDB). Measured isotope values were corrected for variation with sample size. During the period that the samples were measured this correction amounted to ~0.02‰ in $\delta^{13}C$ over the range of 1–9 Volt of signal intensity. However, no correction for scale-compression is needed. Using NBS19 as a single anchor point the measured values for NBS18 were within one standard deviation of the accepted values. Over the interval the samples were run, the mean $\delta^{13}C$ values for standards NBS19 and NBS18 were 1.95‰ and −5.01‰ respectively. The standard deviation of the standard means was < 0.05‰. The external precision (1σ) for $\delta^{13}C$, based on the replicate analyses of the internal standard Carrara marble, over the course of the analyses for this study, was ≤0.05‰.

2.5. Ontogenetic trend analysis

To evaluate if the *G. glycymeris* $\delta^{13}C_{shell}$ data are impacted by ontogenetic processes the annually resolved $\delta^{13}C_{shell}$ data from each individual shell was aligned by ontogenetic age and the mean and standard deviation calculated. This process results in the generation of a mean population $\delta^{13}C_{shell}$ curve relative to shell ontogenetic age. As the shells incorporated in these analyses span a broad time interval, this process averages out the environmentally driven trends, that vary differently across the variety of time intervals represented by the shells, while the common $\delta^{13}C_{shell}$ trends related to shell ontogeny, if present, are preserved as these should remain relatively constant through time. The incorporation of pre-industrial *G. glycymeris* shells in the mean population $\delta^{13}C_{shell}$ curve is also necessary due to the possibility of a

confounding negative $\delta^{13}C_{shell}$ trend recorded in shells representing the industrial era, related to the marine Suess effect (Suess, 1953; Butler et al., 2009; Galbraith et al., 2015; Eide et al., 2017). To evaluate the potential influence of the marine Suess effect on the mean population $\delta^{13}C_{shell}$ curve, the mean population $\delta^{13}C_{shell}$ curve was estimated a total of three times using different suites of shells. The first mean population $\delta^{13}C_{shell}$ curve contained data obtained from all the shells sampled, irrespective of shell antiquity (referred to as $\delta^{13}C_{all-shells}$). The second and third replicate mean population $\delta^{13}C_{shell}$ curves were generated using only shells that derived from the industrial (1800 CE to present) and pre-industrial (pre-1800 CE) time intervals respectively (referred to as $\delta^{13}C_{industrial}$ and $\delta^{13}C_{pre-industrial}$ respectively). To evaluate the number of individual $\delta^{13}C_{shell}$ series required to develop a representative mean population $\delta^{13}C_{shell}$ curve, the standard error or the population $\delta^{13}C_{shell}$ curves were regressed against the corresponding number of shells used to generate the curve (supplementary Fig. 2).

The mean population $\delta^{13}C_{shell}$ curves were initially filtered using a 10-year first order loess low pass filter and the first differential calculated. The low pass filter was used to reduce noise in the data whilst preserving decadal to centennial scale trends. Persistent positive (negative) first differential values were used to identify positive (negative) trends in $\delta^{13}C_{shell}$ values. Based on these data, the non-filtered (annually resolved) mean population $\delta^{13}C_{shell}$ curves were split into two separate time intervals where the $\delta^{13}C_{shell}$ data were characterised by little or no persistent trend and an interval of a persistent negative trend in $\delta^{13}C_{shell}$ respectively. The precise timing of these intervals was defined using the position (ontogenetic age) at which the first differential intercepts the x-axis denoting a change in trend ($\delta^{13}C_{all-shells}$ 1–17 and 18–70; $\delta^{13}C_{industrial}$ 1–11 and 12–70; and $\delta^{13}C_{pre-industrial}$ 1–19 and 20–64 respectively; Fig. 4). Linear and non-linear regression models were then used to evaluate the significance of the trends over each interval.

2.6. Constructing a multi-centennial $\delta^{13}C$ record

Given the maximum longevity of *G. glycymeris* from the Tiree passage is ~200 years (Reynolds et al., 2013), the construction of a multi-centennial to millennial length *G. glycymeris* $\delta^{13}C_{shell}$ record requires combining overlapping $\delta^{13}C_{shell}$ data derived from multiple shells. To estimate the degree of uncertainty that is associated with differences in $\delta^{13}C_{shell}$ between individual shells growing in the same calendar years (referred to as inter-shell $\delta^{13}C_{shell}$ variability) the standard deviation was calculated between $\delta^{13}C_{shell}$ data derived from growth increments formed in the same calendar year across multiple shells. This approach results in the evaluation of inter-shell $\delta^{13}C_{shell}$ variability associated with combining $\delta^{13}C_{shell}$ data from growth increments spanning a range of ontogenetic ages but formed within the same calendar year. Linear regression analyses were used to quantitatively evaluate the influence of combining $\delta^{13}C_{shell}$ data from growth increments of differing ontogenetic ages. These analyses were performed by regressing the inter-shell $\delta^{13}C_{shell}$ variability data against the corresponding standard deviation in ontogenetic age of the growth increments sampled in that given year. In addition, to evaluate if the inter-shell $\delta^{13}C_{shell}$ variability is associated with the absolute ontogenetic age of the growth increments sampled (rather than the difference in ontogenetic age between replicated samples) linear regression analyses were conducted between the inter-shell $\delta^{13}C_{shell}$ variability data and the corresponding mean ontogenetic age of the growth increments sampled.

The $\delta^{13}C_{shell}$ data from each individual shell was detrended using a high pass filter (20 year first order loess filter) to remove possible ontogenetic trends. A 20 year high pass filter was used for two reasons: i) It is a relatively flexible filter and as such accurately adapts to the variable long-term trends in the $\delta^{13}C_{shell}$ data. Applying a stiffer filter (e.g. 40 years) may not accurately follow trends in the $\delta^{13}C_{shell}$ resulting in the detrended $\delta^{13}C_{shell}$ data containing statistical artefacts. ii) Using a

20 year filter results in the minimal loss of $\delta^{13}C_{shell}$ data at either end of the detrended timeseries. As an average of 60 years of data were obtained per shell, using a high pass filter that capture more low frequency variability (e.g. a 40 year high pass filter) would result in a greater proportion of data being lost (at the beginning and end of each shells dataset). Such a loss in data could lead to gaps in the final compiled $\delta^{13}C_{shell}$ dataset. In years represented by multiple replicate samples the arithmetic mean of the detrended annually resolved $\delta^{13}C_{shell}$ data were calculated. The uncertainty associated with the annually resolved $\delta^{13}C_{shell}$ record was derived as the root mean squared error (RMSE) combining the inter-shell $\delta^{13}C_{shell}$ variability, calculated using the detrended data ($1\sigma = 0.07‰$), and the external analytical precision ($1\sigma = 0.05‰$). As the resulting $\delta^{13}C_{shell}$ series generated using all of the detrended annually resolved $\delta^{13}C_{shell}$ data contains only high frequency variability, it is hereafter referred to as the $\delta^{13}C_{high}$ record.

As the detrending process removes low frequency variability, be it of ontogenetic or environmental origin, we used a further approach to construct the long-term $\delta^{13}C_{shell}$ record. As the ontogenetic $\delta^{13}C_{shell}$ analyses indicate there is either no significant or only a small ontogenetic trend in $\delta^{13}C_{shell}$ over the first 20 years of ontogenetic age (see Section 3.2) non-detrended data from only these increments were utilised to quantify low frequency variability not captured by the detrended $\delta^{13}C_{high}$ record. The resulting $\delta^{13}C_{shell}$ series generated using $\delta^{13}C_{shell}$ data derived from growth increments < 20 years of age is hereafter referred to as the $\delta^{13}C_{low}$ record. The uncertainty associated with the $\delta^{13}C_{low}$ record was derived as RMSE combining the inter-shell $\delta^{13}C_{shell}$ variability, calculated using the annually resolved $\delta^{13}C_{shell}$ data derived from the first 20 growth increments replicated over multiple shells ($1\sigma = 0.11‰$), and the external analytical $\delta^{13}C$ precision ($1\sigma = 0.05‰$).

The trends captured by the $\delta^{13}C_{low}$ record were evaluated using linear model analyses. The nature of the variability contained in the annually resolved $\delta^{13}C_{high}$ record was assessed using Mortlet wavelet analysis. The linear model and wavelet analysis were carried out using Past V3.

2.7. Environmental analysis

The $\delta^{13}C_{high}$ and $\delta^{13}C_{low}$ records provide an opportunity to evaluate if the ontogenetic related fractionation processes mask the $\delta^{13}C_{shell}$ variability related to environmental change. To test if this is the case, both the $\delta^{13}C_{high}$ and $\delta^{13}C_{low}$ records were correlated against spatial and temporal oceanographic timeseries over the interval 1954–2010 CE and the strength of the resulting correlations compared.

Point correlations were calculated between the annually resolved $\delta^{13}C_{high}$ and $\delta^{13}C_{low}$ records and gridded sea surface temperature (SST; HadISST1; Rayner et al., 2003) and sea surface salinity (SSS; EN4 SSS; Good et al., 2013) data products to assess if physical environmental factors play a role in driving $\delta^{13}C_{shell}$ variability. Comparison between the $\delta^{13}C_{high}$ and $\delta^{13}C_{low}$ records and environmental data were conducted using linear detrended data. The data were detrended to mitigate the influence of the negative trend in $\delta^{13}C$ associated with the marine Suess Effect, which is not climatically driven. The point correlations were conducted using KNMI Climate Explorer (http://climexp.knmi.nl Trouet and Van Oldenborgh, 2013). Correlations were calculated over the interval 1954 to 2010 CE. To provide a quantitative assessment of the significance of the relationships identified by the point correlation analyses linear regression analyses were conducted between the *G. glycymeris* $\delta^{13}C_{high}$ and $\delta^{13}C_{low}$ records and SST and SSS data obtained from the gridded data products from a grid box centred on the Tiree Passage and Sea of the Hebrides (50–60°N by 3–10°W). In addition, given that $\delta^{13}C_{shell}$ variability has previously been associated with variability in primary productivity, linear regression analyses were conducted between the $\delta^{13}C_{high}$ and $\delta^{13}C_{low}$ records and primary productivity data from the 55–60°N by 3–10°W grid box from the

Continuous Plankton Recorder (CPR) survey data set (https://www.sahfos.ac.uk/) as well as available river flow data from northwest Scotland (https://nrfa.ceh.ac.uk/data). Multiple linear regression analyses were used to evaluate the cumulative coherence that these environmental parameters share with the $\delta^{13}C_{shell}$ data. Multiple linear regression was carried out in RStudio V1.1.456.

2.8. Multi-proxy analysis

Running correlations were calculated between the $\delta^{13}C_{high}$ data and the Tiree Passage *G. glycymeris* $\delta^{18}O_{shell}$ and growth increment width series. Correlations were calculated over a 30 year running window with 29 years of overlap. Due to the gaps in the $\delta^{13}C_{low}$ data set these data were not used in the running correlation analysis. To take into account the fact that the $\delta^{13}C_{high}$ and growth increment width series were constructed from detrended data, the $\delta^{18}O_{shell}$ series were detrended using a first order loess high pass filter. The application of the detrending to the $\delta^{18}O_{shell}$ provides for a like for like comparison between the $\delta^{13}C_{high}$, $\delta^{18}O_{shell}$ and growth increment width series. Principal component analysis (PCA) was used to evaluate the common signal contained by the $\delta^{13}C_{high}$, $\delta^{18}O_{shell}$ and growth increment width series. The PCA was calculated over the entire common period contained by the three records and the primary principal component extracted. Finally, the $\delta^{13}C_{high}$, $\delta^{13}C_{low}$, primary principal component from the PCA were calibrated against instrumental salinity data derived from the EN4 SSS dataset. These data were then converted to $\delta^{18}O_w$ using the local salinity mixing line equation (Cage and Austin, 2010). The resulting reconstructed $\delta^{18}O_w$ data were then independently integrated with the $\delta^{18}O_{shell}$ data, using the Grossman and Ku (1986) aragonite palaeotemperature equation. The resulting reconstructed seawater temperatures were compared using linear regression analysis and the associated mean squared errors calculated.

3. Results and discussion

3.1. Shell dating

The dates of the samples derived from the modern (industrial period) shells were based on the Tiree Passage *G. glycymeris* master growth increment width sclerochronology (Reynolds et al., 2013). The AMS ^{14}C determinations of the fossil *G. glycymeris* shells that did not crossdate into the master sclerochronology identified a broad range of dates (Supplementary Fig. 3 and Supplementary Table 1). The calibrated ^{14}C ages of the 21 shells spanned from 116 to 8755 years BP.

3.2. Ontogenetic analysis

The mean population $\delta^{13}C_{all-shells}$ curve was constructed from $\delta^{13}C_{shell}$ data derived from 1745 unique growth increments sampled at annual resolution across 26 individual shells (Fig. 2). The mean population $\delta^{13}C_{industrial}$ curve was constructed from $\delta^{13}C_{shell}$ data derived from 476 unique growth increments sampled at annual resolution across seven individual shells. An average of 59.5 (range of 18 to 142) samples were taken per shell over the industrial era. The mean population $\delta^{13}C_{pre-industrial}$ curve was constructed from $\delta^{13}C_{shell}$ data derived from 1269 unique growth increments sampled at annual resolution from a total of 18 individual shells. A mean of 70.5 (range of 23 to 114) samples were taken per shell over the pre-industrial era.

Examination of the standard error of the mean population $\delta^{13}C_{all-shell}$ curve verses the number of shells used to construct the population curve (sample depth; Fig. S1) shows a negative trend in both the mean standard error and in the standard deviation of the standard error with increasing sample depth. The standard deviation of the standard errors stabilises at a sample depth > 7 individual shells per year (mean standard error of 0.1‰) suggesting this is the minimum replication required to produce a representative population $\delta^{13}C_{shell}$ curve.

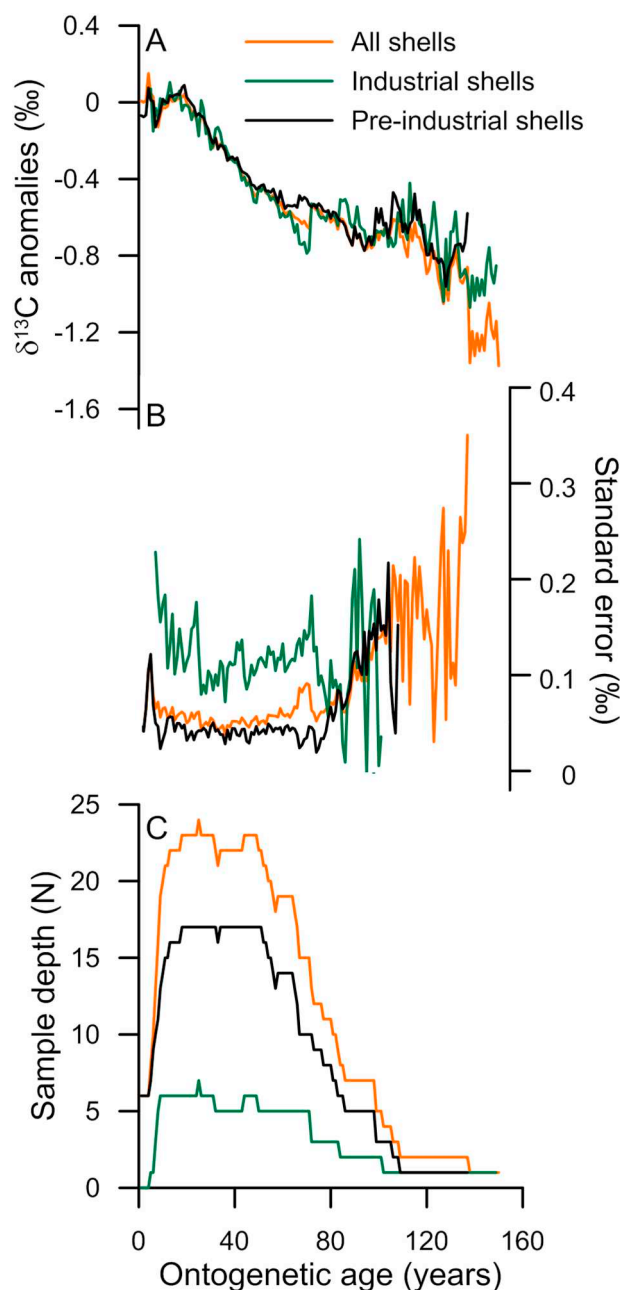**Fig. 2.** Comparison between the three mean population $\delta^{13}C$ curves ($\delta^{13}C_{high\ shells}$ = orange line; $\delta^{13}C_{industrial}$ = green line; and $\delta^{13}C_{pre-industrial}$ = black line). Anomalies calculated relative to the mean of the first 20 years of the raw population $\delta^{13}C_{shell}$ curve. Panels B and C show the standard error and sample depth data for the each of the corresponding population $\delta^{13}C_{shell}$ curves respectively. (For interpretation of the references to colour in this figure legend, the reader is referred to the web version of this article.)

Intervals of the mean population $\delta^{13}C_{shell}$ curves with a sample depth < 7 shells per year therefore contain increased levels of uncertainty and may not accurately reflect population trends in $\delta^{13}C_{shell}$. Fig. 2B shows the sample depth and standard error for the three mean population $\delta^{13}C_{shell}$ curves over the first 80 years of ontogenetic age and highlights the low standard errors associated with the $\delta^{13}C_{all-shells}$ and $\delta^{13}C_{pre-industrial}$ mean population $\delta^{13}C_{shell}$ curves (each > 7 shell per year sample depth over this interval) compared to the $\delta^{13}C_{industrial}$ mean population curve that has a sample depth < 7 shells per year. The standard error in all three mean population $\delta^{13}C_{shell}$ curves increases after approximately 70 years.
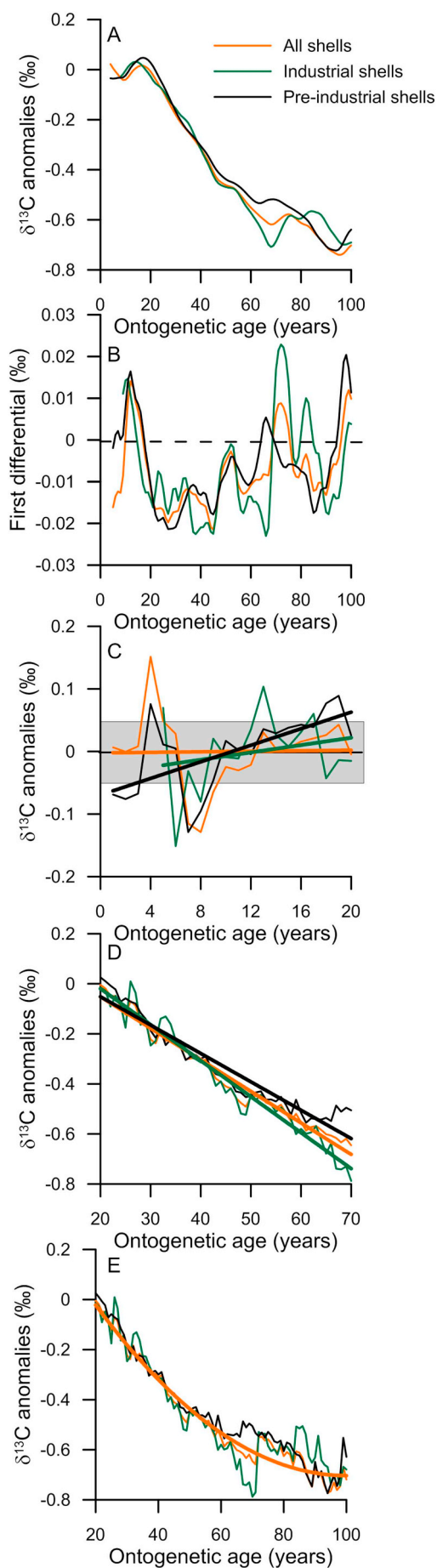
Fig. 3. A) Ten year first order loess low pass filtered mean population δ^{13}C curves ($\delta^{13}C_{all\_shells}$ = orange line; $\delta^{13}C_{industrial}$ = green line; and $\delta^{13}C_{pre-industrial}$ = black line). Anomalies calculated relative to the mean of the first 20 years of the raw population $\delta^{13}C_{shell}$ curve. B) The first differential of the 10 year first order loess low pass filtered mean population δ^{13}C curves. The dashed black line denotes the zero-line representing the transition between positive and negative trends in the mean population $\delta^{13}C_{shell}$ curves. C) Data from the first 20 years of the mean population δ^{13}C curves (thin lines) fitted with linear models (thick lines). The shaded grey box denotes the ± 0.05‰ δ^{13}C analytical precision. D) Linear model analysis (thick lines) of the mean population δ^{13}C curves (thin lines) derived over the interval 20–70 years of age. E) The mean population δ^{13}C curves plotted over the interval 20–100 years of age (thin lines) fitted with a second order polynomial model (thick lines). The $\delta^{13}C_{shell}$ data are plotted as anomalies relative to the mean of the $\delta^{13}C_{all-shells}$ series calculated over the first 20 years of ontogenetic age. (For interpretation of the references to colour in this figure legend, the reader is referred to the web version of this article.)

The 10-year first order loess low pass filtered mean population $\delta^{13}C_{shell}$ curves and corresponding first differential data highlights consistent trends across all three curves (Fig. 3). These data highlight two key intervals in the $\delta^{13}C_{shell}$ data. The first ~20 years, where the $\delta^{13}C_{shell}$ curves are relatively flat, and between 20 and 70 years of ontogenetic age where the data are characterised by persistent negative trends in $\delta^{13}C_{shell}$. After 70 years of age the three mean population $\delta^{13}C_{shell}$ curves continue to exhibit a potential reduction in $\delta^{13}C_{shell}$ however the mean population $\delta^{13}C_{shell}$ curves contain reduced sample depth over this interval.

No significant linear trends are found over the first 20 years of ontogenetic age in the $\delta^{13}C_{all-shells}$ and $\delta^{13}C_{industrial}$ mean population $\delta^{13}C_{shell}$ curves (Fig. 3C and Table 1). However, the $\delta^{13}C_{pre-industrial}$ mean population curve does contain a significant positive trend (0.007‰ yr^{-1}, 95% bootstrapped confidence interval 0.003 to 0.010‰ yr^{-1}). Between 20 and 70 years of ontogenetic age all three mean population $\delta^{13}C_{shell}$ curves exhibit highly significant (P < 0.001) linear decreases in $\delta^{13}C_{shell}$ (−0.013‰ yr^{-1}, −0.014‰ yr^{-1} and -0.011‰ yr^{-1} for the $\delta^{13}C_{all-shells}$, $\delta^{13}C_{industrial}$ and $\delta^{13}C_{pre-industrial}$ mean population $\delta^{13}C_{shell}$ curves respectively; Fig. 3D and Table 1B). As the sample depth in the $\delta^{13}C_{all-shells}$ mean population curve remains ≥7 shells per year up to 98 years of ontogenetic age, these data provide an assessment of somewhat longer trends (Fig. 3C). After ~70 years of ontogenetic age the $\delta^{13}C_{all-shells}$ mean population $\delta^{13}C_{shell}$ curve data suggests a shift away from the negative linear trend observed in the 20–70 years of ontogenetic age interval (Fig. 3E). This is represented by a second order polynomial fit (R = 0.98 P < 0.001; Fig. 3E and Table 1C). Whilst the sample depth remains < 7 shells per year in both the $\delta^{13}C_{industrial}$ and $\delta^{13}C_{pre-industrial}$ mean population $\delta^{13}C_{shell}$ curves, second order polynomial models can explain 89% and 96% (P < 0.001) of the variability in the data derived from growth increments between 20 and 100 years of ontogenetic age respectively (Table 1C).

The identification of negative δ^{13}C trends in *G. glycymeris* $\delta^{13}C_{shell}$ data is consistent with results of the analysis of other marine bivalves that exhibit a similar decline in $\delta^{13}C_{shell}$ with ontogenetic age (e.g. *Pecten maximus* (Lorrain et al., 2004), *Mercenaria mercenaria* (Gillikin et al., 2007), *Spisula solidissima* (Krantz et al., 1987), *Placopecten magellanicus* (Keller et al., 2002), *Pinna nobilis* (Kennedy et al., 2001) and *Chamelea gallina* (Keller et al., 2002)). The magnitude of $\delta^{13}C_{shell}$ ontogenetic trends previously recorded ranges from ca. 0.5‰ in the first few growth increments of *A. islandica* (Reynolds et al., 2017a) up to 4‰ in *M. mercenaria* (Gillikin et al., 2007). The shift of up to ca. 0.7‰ in *G. glycymeris* is therefore in line with other marine bivalves that exhibit ontogenetic related trends in $\delta^{13}C_{shell}$.

Whilst our study provides no indication of the mechanism that drives the observed negative ontogenetic trend in $\delta^{13}C_{shell}$, given that the generation of our mean population $\delta^{13}C_{all-shells}$ and $\delta^{13}C_{pre-industrial}$ curves integrate shell material that span the Holocene, at sufficient

Table 1
A-B) Results of the linear regression modelling to evaluate the significance of the trends in the three mean population $\delta^{13}C$ curves over A) the first 20 years of ontogenetic age and B) 20–70 years of ontogenetic age. C) Results of the non-linear (second order polynomial) model analysis of the $\delta^{13}C$ data derived from growth increments between 20 and 100 years of ontogenetic age.

A

Linear model of $\delta^{13}C$ data derived from first 20 years of ontogenetic age

	Slope (‰ yr^{-1})	95% CI (‰ yr^{-1})	r	R^2	t	p
All shells	0.000	-0.004, 0.004	0.02	0.00	0.09	0.93
industrial shells	0.003	-0.005, 0.01	0.25	0.06	0.95	0.36
Pre industrial	0.007	0.003, 0.010	0.65	0.42	3.61	<0.01

B

Linear model of $\delta^{13}C$ data derived from growth increments of 20-70 years of ontogenetic age

	Slope (‰ yr^{-1})	95% CI (‰ yr^{-1})	r	R^2	t	p
All shells	-0.013	-0.013, -0.012	-0.99	0.97	-40.82	<0.0001
industrial shells	-0.014	-0.015, -0.013	-0.98	0.96	-32.74	<0.0001
Pre industrial	-0.011	-0.012, -0.010	-0.96	0.93	-24.64	<0.0001

C

Non-linear model of $\delta^{13}C$ data derived from growth increments 20-100 years of ontogenetic age

	Chi^2	R^2	F:	p:	Equation
All shells	0.12	0.97	1127.00	<0.001	$Y = 0.0001064x^2 - 0.0213x + 0.3619$
industrial shells	0.38	0.89	326.70	<0.001	$Y = 0.0001542x^2 - 0.0264x + 0.4774$
Pre industrial	0.15	0.96	852.34	<0.001	$Y = 9.553E\text{-}05x^2 - 0.01978x + 0.3459$

sample depth to facilitate the generation of a significant mean population $\delta^{13}C_{shell}$ curve, it is highly unlikely that the negative trend in $\delta^{13}C_{shell}$ originates from an environmental source such as the marine Suess effect. Previous studies argue that ontogenetic trends in $\delta^{13}C_{shell}$ data derived from marine molluscs likely stem from a relative increase in the proportion of metabolic CO_2 incorporated into the shell carbonate with age (Lorrain et al., 2004; Gillikin et al., 2007; McConnaughey and Gillikin, 2008). Marine bivalves typically incorporate ca. 10% of respired and metabolic CO_2 into shell carbonate (Goodwin et al., 2013). Species that exhibit negative ontogenetic trends in $\delta^{13}C_{shell}$ have been reported to increase the proportion of respired/metabolic CO_2 incorporated into the shell up to a total of as much as 37% (Gillikin et al., 2007). Given the $\delta^{13}C$ of marine phytoplankton is typically -20‰ to -30‰ (Mook and Tan, 1991), increasing the relative proportion of carbon derived from this source, in the form of metabolic and respired CO_2, would drive a strong response in the $\delta^{13}C_{shell}$ composition of the shell (Lorrain et al., 2004; Gillikin et al., 2007; Goodwin et al., 2013).

3.3. Constructing a multi-centennial $\delta^{13}C$ series

Given that significant ontogenetic trends were found in the annually resolved *G. glycymeris* $\delta^{13}C_{shell}$ data it was important to evaluate the influence these trends would have on the resulting record constructed from $\delta^{13}C_{shell}$ data derived from growth increments of differing ontogenetic ages. In total there were 182 years containing replicated data between independent shells. Unsurprisingly, a significant positive linear correlation was found between inter-shell $\delta^{13}C_{shell}$ variability and the standard deviation in ontogenetic age of the growth increments sampled ($R = 0.76$, $P < 0.01$; slope = 0.006‰ yr^{-1}, 95% CI 0.002‰ yr^{-1} to 0.011‰ yr^{-1}, $N = 182$; Fig. 4). This result suggests that failure to remove the ontogenetic trend will result in the final $\delta^{13}C_{shell}$ record containing large uncertainties. However, no significant correlations were found between (i) inter-shell $\delta^{13}C_{shell}$ variability and mean ontogenetic age of the increments sampled ($R = -0.04$, $P = 0.53$, $N = 182$; Fig. 4B); (ii) the linear detrended inter-shell $\delta^{13}C_{shell}$ variability and

standard deviation in ontogenetic age of the increments sampled ($R = -0.11$, $P = 0.65$, $N = 182$); or (iii) the linear detrended inter-shell $\delta^{13}C_{shell}$ variability and the mean ontogenetic age of the increments sampled ($R = 0.01$, $P = 0.86$, $N = 182$). Importantly there was also no significant trend found between the number of sub-annual resolution samples used to calculate the annual resolution $\delta^{13}C_{shell}$ value and the resulting incremental mean $\delta^{13}C_{shell}$ value (Fig. 4C). These data suggest that, despite the likely high amplitude of sub-annual environmental $\delta^{13}C$ variability, taking either a single sample per year, or taking the arithmetic mean of multiple sub-annual $\delta^{13}C_{shell}$ values results in a reproduceable annually resolved $\delta^{13}C_{shell}$ data. These data therefore suggest that incorporating undetrended data from the earliest growth increments < 20 years, or using detrended $\delta^{13}C_{shell}$ data, results in the construction of a long-term $\delta^{13}C_{shell}$ series that contain consistent inter-shell $\delta^{13}C_{shell}$ variability and therefore uncertainty.

Previous studies have demonstrated that detrending $\delta^{13}C$ data that contain ontogenetic trends can effectively remove the ontogenetic signal in $\delta^{13}C$ data (Chauvaud et al., 2011). Investigating the impact of detrending the $\delta^{13}C_{shell}$ data on the inter-shell $\delta^{13}C_{shell}$ variability indicates that applying detrending techniques such as linear detrending or high pass filtering effectively removes the ontogenetic effects and results in the generation of an annually resolved *G. glycymeris* $\delta^{13}C$ series with mean inter-shell $\delta^{13}C_{shell}$ variability of 0.07‰. Whilst detrending the $\delta^{13}C_{shell}$ data effectively removes the ontogenetic trend in $\delta^{13}C_{shell}$ the detrending process also removes low frequency variability not associated with the ontogenetic trend, i.e. environmental variability (Cook et al., 1995). As such the $\delta^{13}C_{high}$ series constructed using detrended $\delta^{13}C_{shell}$ records would be constrained to examining high frequency (inter-annual to multi-decadal) variability in marine carbon dynamics.

Considerable effort has been made in the fields of dendrochronology and sclerochronology to investigate alternative detrending techniques that can preserve a greater proportion of low frequency variability (e.g. Cook et al., 1995; Wigley et al., 1987; Esper et al., 2002). One such approach is the use of regional curve standardisation (RCS; Esper et al.,
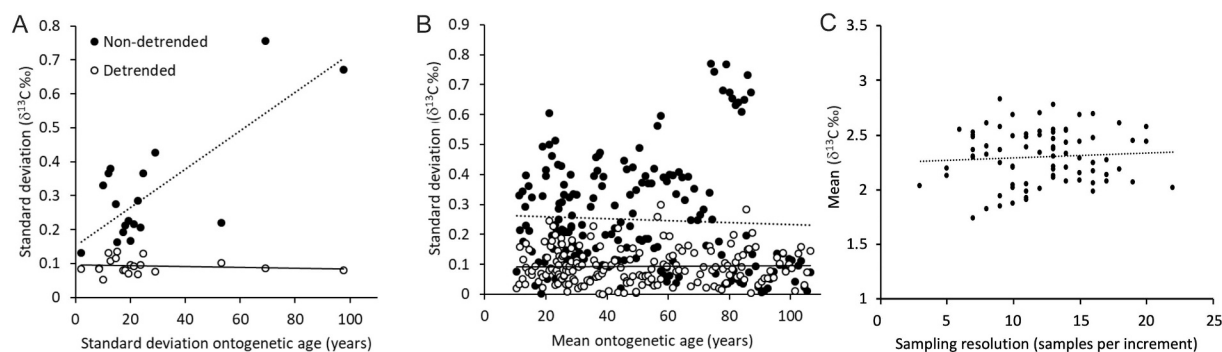
Fig. 4. A) Weighted mean inter-shell $\delta^{13}C_{shell}$ variability plotted against the standard deviation of the ontogenetic age of the increments sampled in that given year. In panels A and B, the solid black circles denote non-detrended data whilst the unfilled black circles denote linear detrended data. Given the heterogeneous distribution of the data weighted mean standard deviations are plotted. B) Inter-shell $\delta^{13}C$ variability plotted against the mean ontogenetic age of the increments sampled. In panels A and B the dashed black line and solid black lines denote the line of best fit for the non-detrended and linear detrended data respectively. C) Linear regression analysis between the number of sub-annually resolved $\delta^{13}C_{shell}$ samples used to generate the annual mean $\delta^{13}C_{shell}$ value and the corresponding mean $\delta^{13}C_{shell}$ value.

2002). Whilst RCS detrending is more commonly known for its application in detrending growth increment series, RCS has previously been applied to remove ontogenetic $\delta^{13}C$ trends in *Pinus sylvestris* (Gagen et al., 2008). The application of RCS detrending has been demonstrated to be more effective at preserving low frequency variability than linear or spline detrending techniques (Esper et al., 2002). However, the generation of a robust RCS curve requires data from a substantial number of individual shells (typically > 60; Esper et al., 2002). Whilst the mean population $\delta^{13}C_{shell}$ curve presented here contains sufficient replication to provide a statistical assessment of the ontogenetic trends in the $\delta^{13}C_{shell}$ data, over the first 70 years, it does not contain sufficient replication to be utilised as an RCS curve. At this stage therefore, the application of RCS detrending techniques does not present a viable option for removing the ontogenetic trends in *G. glycymeris* $\delta^{13}C_{shell}$ data. However, as the ontogenetic $\delta^{13}C_{shell}$ analyses indicate that the $\delta^{13}C_{low}$ data contain no (or only very weak) ontogenetic trends, it is possible that these data provide an annually resolved $\delta^{13}C_{shell}$ series that would facilitate the investigation of low-frequency variability (Fig. 5C). Such an approach would increase the combined RMSE uncertainty to ± 0.12‰ of the timeseries, as the inter-shell $\delta^{13}C_{shell}$ variability in the non-detrended $\delta^{13}C_{low}$ data is slightly higher than the corresponding detrended data (0.11‰ compared to 0.07‰). Additionally, only utilising growth increments < 20 years of age would potentially impact the ability to generate long-term continuous records as the sample depth of such increments is not uniform throughout the master chronology used as the temporal framework for the $\delta^{13}C_{shell}$ analyses. Portions of the master growth increment width chronology that contain no growth increments < 20 years of age would therefore not be represented in the series and this would result in a non-continuous record. This potential complication could be mitigated by the inclusion of significant numbers of additional shells within the master sclerochronology.

The mean detrended (non-detrended) inter-shell $\delta^{13}C_{shell}$ variability (1σ), calculated using $\delta^{13}C_{shell}$ data derived from 473 unique growth increments spanning 185 individual years over the industrial era is 0.07‰ (0.3‰). The mean detrended (non-detrended) inter-shell $\delta^{13}C_{shell}$ variability derived from the growth increments < 20 years of ontogenetic age, replicated across 41 increments in 19 unique years and eight individual shells, is 0.07‰ (0.11‰). Combining these uncertainties with the analytical precision of ± 0.05‰, the root mean squared error (RMSE) for the annually resolved records are 0.09‰ and 0.12‰ for the $\delta^{13}C_{high}$ and $\delta^{13}C_{low}$ series respectively.

As expected, the annually resolved $\delta^{13}C_{high}$ record contains no variability with periodicities > 20 years and no long-term trends (Fig. 5 and Supplementary Fig. S4). However, wavelet analyses indicate that there is significant variability (P < 0.05) in the $\delta^{13}C_{high}$ record at periodicities ranging from 8 to 20 years (Supplementary Fig. 5). In

contrast, the $\delta^{13}C_{low}$ record contains a significant negative trend over the interval from 1939 to 2010 CE (slope = −0.014‰ yr^{-1}; 95% CI range of −0.015 to −0.012‰ yr^{-1}; R = 0.93, P < 0.0001, N = 71). Over the interval from 1799 to 1939 CE the $\delta^{13}C_{low}$ record contains a weak but significant negative trend of −0.001‰ yr^{-1}; 95% CI range of −0.002 to −0.0005‰ yr^{-1}; R = 0.47, P < 0.01, N = 140). Comparison of the $\delta^{13}C_{low}$ data with corresponding data derived from the three *A. islandica* shells analysed (spanning 1944 to 1962 CE) shows good coherence (Fig. 5C). Mean standard deviation calculated between the *G. glycymeris* and *A. islandica* $\delta^{13}C_{shell}$ data replicated in the same calendar years is ± 0.1‰ (1σ). While the trend captured by the *A. islandica* data (−0.017 ± 0.04‰ yr^{-1}) is identical to the long-term trend in the *G. glycymeris* $\delta^{13}C_{low}$ record over the same interval (−0.017 ± 0.005‰ yr^{-1}).

Whilst there is variability in the amplitude of the trends, previously published sclerochronologically derived $\delta^{13}C_{shell}$ records have demonstrated that the $\delta^{13}C_{DIC}$ in the North Atlantic over the 20th century reflects the reduction in $\delta^{13}C$ associated with the marine Suess Effect (Reynolds et al., 2017a; Butler et al., 2009; Schöne et al., 2011; Wanamaker Jr. et al., 2011). Similarly in Loch Sunart, a sea loch adjacent to the Tiree Passage, benthic foraminiferal $\delta^{13}C$ has shown a particularly pronounced decrease in $\delta^{13}C$ over the latter half of the 20th century (Cage and Austin, 2010). Comparison of these data with the low frequency variability contained in our discontinuous $\delta^{13}C_{low}$ record highlights a broadly consistent picture. Whilst during the 19th century the burning of fossil fuels initiated a significantly negative trend in $\delta^{13}C$ of atmospheric CO_2 ($\delta^{13}C_{atm}$; Francey et al., 1999) both the Loch Sunart and $\delta^{13}C_{low}$ data contain no signficant trend over this interval (Fig. 5). However, both the Loch Sunart and $\delta^{13}C_{low}$ data contain significant negative trends in $\delta^{13}C$ over the latter half of the 20th century. Whilst the discontinuous nature of the $\delta^{13}C_{low}$ data prevents the identification of the precise date of the onset of the negative trend, the examination of the Loch Sunart record suggests the negative trend began ca. 1900 (Cage and Austin, 2010). Observed and reconstructed $\delta^{13}C_{atm}$ data contain trends over the latter half of the 20th century of −0.29‰ yr^{-1} and -0.02‰ yr^{-1} respectively (Francey et al., 1999). However, the $\delta^{13}C_{low}$ data contain a trend of −0.013‰ yr^{-1}, which is broadly in line with other marine proxy records of the marine Suess effect over the period from 1950 to 2000 (North Iceland: −0.013‰ yr^{-1} (Reynolds et al., 2017a, Schöne et al., 2011) −0.011‰ yr^{-1} (Schöne et al., 2011); Isle of Man −0.14‰ yr^{-1} (Butler et al., 2009); Gulf of Maine −0.007‰ yr^{-1} (Wanamaker et al., 2008a; Schöne et al., 2011)). However, closer examination of the trends present in the $\delta^{13}C_{low}$ data and these contemporaneous $\delta^{13}C$ records over the instrumental period highlights there are differences in higher frequency variability between these locations (Supplementary Table 2). Such differences are likely due to differences in local hydrography (water masses) and primary
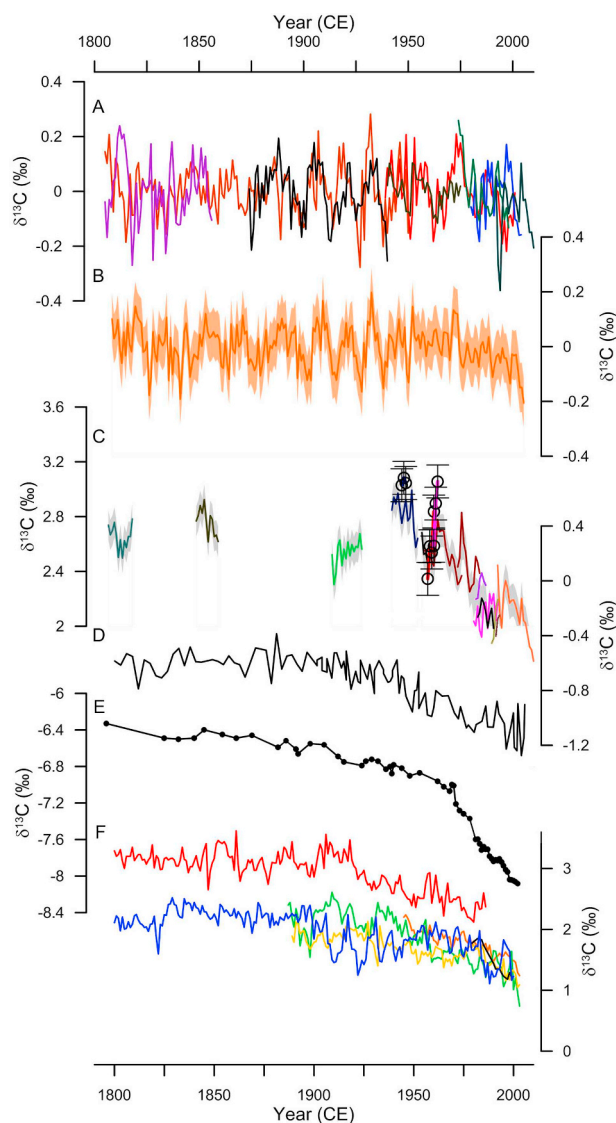
Fig. 5. A) 20 year high pass filtered $\delta^{13}C_{shell}$ data derived from individual *G. glycymeris* shells (represented by different coloured lines) spanning the period 1799–2010 CE. B) The mean annually resolved *G. glycymeris* $\delta^{13}C_{high}$ record (orange line), constructed using the 20 year high pass filtered $\delta^{13}C_{shell}$ data plotted in panel A, plotted with a mean root squared error envelope (RMSE; shaded orange area). The RMSE envelope takes into account mean inter-shell $\delta^{13}C_{shell}$ variability (0.07‰) and analytical precision (0.05‰). C) Plot of the non-detrended $\delta^{13}C_{low}$ data derived from growth increments formed over the first 20 years of ontogenetic age (data from each shell is plotted as a different colour). The black circles represent $\delta^{13}C_{shell}$ data derived from three *A. islandica* shells fitted with RMSE error bars. D) The Loch Sunart $\delta^{13}C_{foram}$ record derived from foraminifera (Cage and Austin, 2010). E) Atmospheric $\delta^{13}C$ composition of CO_2 (Francey et al., 1999). F) Annual resolution $\delta^{13}C$ data derived from *A. islandica* shells from Iceland (Schöne et al., 2011; Reynolds et al., 2017a), the Gulf of Maine (Wanamaker Jr. et al., 2011) and an instrumental $\delta^{13}C$ series (Keeling and Guenther, 1994).

productivity dynamics.

3.4. Environmental analyses

Analyses of the *G. glycymeris* $\delta^{13}C_{shell}$ data against gridded environmental data indicate that the $\delta^{13}C_{low}$ and $\delta^{13}C_{high}$ series correlate significantly with SSS variability in the continental shelf seas west of the UK and Ireland over the time interval 1954–2010 ($R = 0.31$ $P < 0.1$ and 0.50 $P < 0.05$ for the $\delta^{13}C_{high}$ and $\delta^{13}C_{low}$ series

respectively, $N = 56$; Fig. 6). Additionally, these analyses indicate there is no significant correlation between either the $\delta^{13}C_{high}$ or $\delta^{13}C_{low}$ series and SST variability over this region (Fig. 6). This, rather intriguingly, hints at a potential use of *G. glycymeris* $\delta^{13}C_{shell}$ data to help identify the influence of seawater salinity recorded in $\delta^{18}O_{shell}$ reconstructions and isolate the influence of changing seawater temperatures (Gillikin et al., 2006). This would provide an important opportunity to reduce uncertainties associated with annually resolved long-term SST reconstructions based on $\delta^{18}O_{shell}$ data.

Prior to *G. glycymeris* $\delta^{13}C_{shell}$ data being used as a proxy for salinity the mechanisms that link salinity and *G. glycymeris* $\delta^{13}C_{shell}$ must, ideally, first be understood. There are several potential plausible mechanisms. Salinity variability in the Sea of the Hebrides is dictated by the combined influence of North Atlantic waters from the ESC, coastal current waters of the SCC and terrestrial run off and riverine inputs (Inall et al., 2009; Marsh et al., 2017). Changes in the proportion of North Atlantic Ocean water entrained onto the Hebridean shelf have been shown to drive coherent changes in nutrient composition, primary production, temperature and salinity variability across this region (Jickells, 1998). However, these factors have also been shown to drive shifts in $\delta^{13}C_{DIC}$ (Olsen and Ninnemann, 2010; Eide et al., 2017). It is therefore possible that salinity variability is either a primary driver of $\delta^{13}C_{shell}$ variability (via internal fractionation processes), a secondary driver (by driving $\delta^{13}C_{shell}$ variability in association with driving changes in primary productivity), or a combination of mechanisms.

A plausible mechanism has previously been proposed for the direct link between salinity variability and $\delta^{13}C_{shell}$ variability in other marine bivalve molluscs. Gillikin et al. (2006, and references therein) suggest that the enzyme carbonate anhydrase, which catalyses the reaction of bicarbonate to CO_2, can lead to fractionation of the carbon in the carbon pool used to precipitate the carbonate molluscan shell. Furthermore, changes in seawater salinity can lead to enhanced activity of the carbonate anhydrase in molluscan species that osmoregulate (Henry and Saintsing, 1983). Whilst to the best of our knowledge there are no studies of activity of carbonate anhydrase in *G. glycymeris*, the species is known osmoregulate (Gilles, 1972) and thus there remains the potential for carbonate anhydrase to influence the $\delta^{13}C$ composition of the shell.

Whilst the current data preclude the direct assessment of the role salinity plays as a primary driver of $\delta^{13}C_{shell}$ variability, the availability of river flow and primary productivity data, in addition to the local SSS data, provides an opportunity to evaluate the role of salinity as a secondary driver of $\delta^{13}C_{shell}$ variability. Linear regression analyses highlight significant positive correlations between the $\delta^{13}C_{high}$ and $\delta^{13}C_{low}$ records and mean winter river flow ($R = 0.29$ and $R = 0.35$ respectively, $P < 0.1$, $N = 39$). The linear regression analyses also indicate a significant correlation with variability in the $\delta^{13}C_{low}$ record and mean spring river flow. However, unlike during winter, the correlation is negative ($R = -0.26$, $P < 0.1$, $N = 39$). Linear regression analysis between the $\delta^{13}C_{high}$ and $\delta^{13}C_{low}$ records and biological productivity variability in the CPR dataset highlight broadly consistent results. Significant negative correlations were identified between the $\delta^{1}C_{high}$ and $\delta^{13}C_{low}$ records and mean annual primary production ($R = -0.54$ and $R = -0.38$, $P < 0.05$, $N = 39$ respectively; Fig. 7). However, interestingly, the peak correlation between the $\delta^{13}C_{high}$ record and primary production occurs with mean winter variability ($R = -0.60$, $P < 0.05$, $N = 39$).

The correlations identified between primary productivity and the *G. glycymeris* $\delta^{13}C_{shell}$ data are consistent with an increase (decrease) in primary productivity leading to a reduction (increase) in $\delta^{13}C_{DIC}$ (Lynch-Stieglitz et al., 1995). Similar trends have been observed in other marine bivalves such as *A. islandica* (Schöne et al., 2005; Reynolds et al., 2017a). Examination of the correlations between river flow, salinity, primary productivity and the *G. glycymeris* $\delta^{13}C_{shell}$ data suggests that the coherence of the *G. glycymeris* $\delta^{13}C_{shell}$ data with salinity and primary productivity are likely independent. For example, the only significant correlation found in these data between salinity and primary
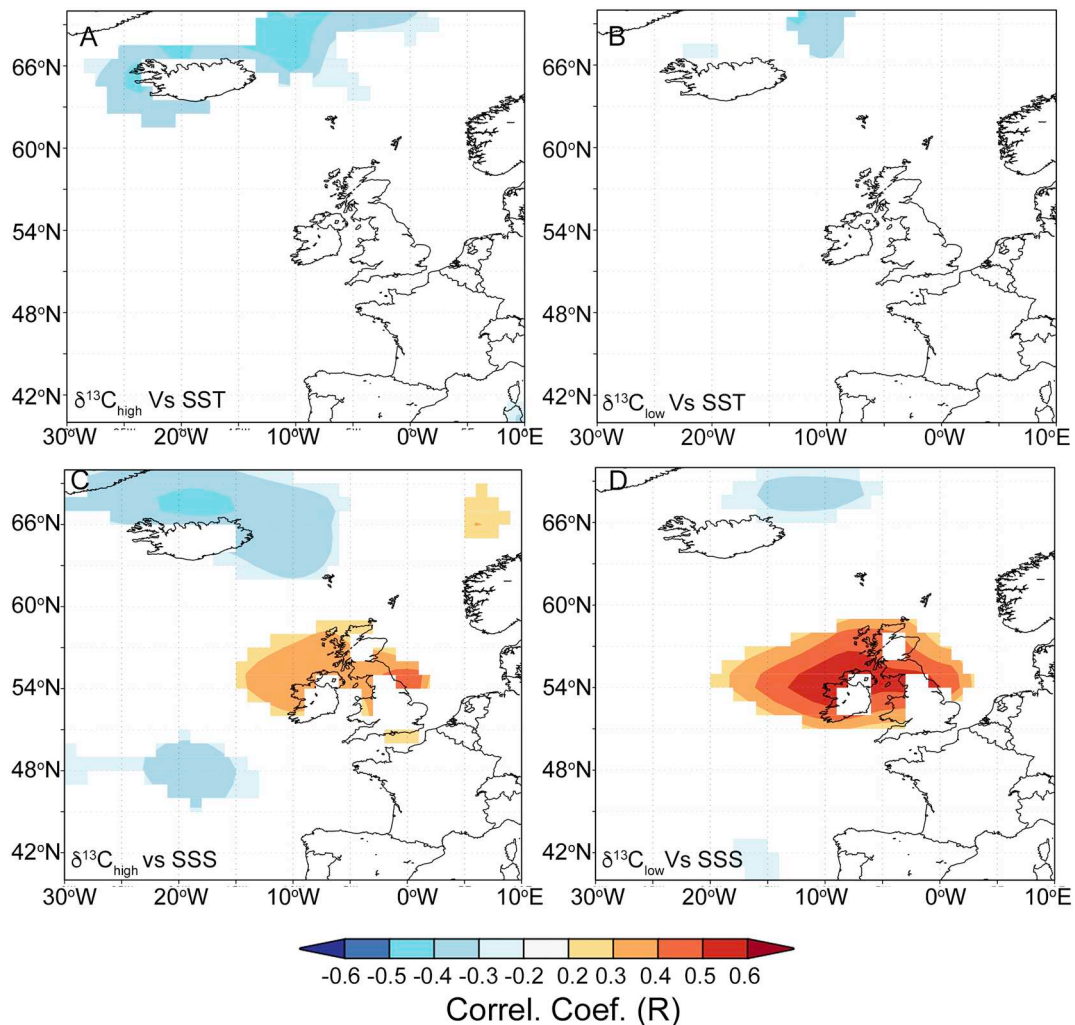
Fig. 6. Point correlations calculated between the $\delta^{13}C_{high}$ (A and C) and (B and D) $\delta^{13}C_{low}$ and instrumental (A and B) HadISST1 SSTs and (C and D) EN4 SSS. Correlations calculated over the period 1954–2010 using linear detrended data. Correlations highlighted are signficant at P < 0.1 level. Correlation analysis conducted using KNMI Climate Explorer.

productivity was with mean summer values (P < 0.1; Supplementary Fig. 5). As this correlation is positive, it would suggest that the impact of an increasing salinity would be an increase in primary production that would lead to a decrease in $\delta^{13}C_{DIC}$. If this were the mechanism that links salinity to *G. glycymeris* $\delta^{13}C_{shell}$ variability, one might therefore expect to see a positive correlation between the *G. glycymeris* $\delta^{13}C_{shell}$ data and primary productivity data, where there is in fact a significant negative correlation.

Given the likely role of multiple factors in driving *G. glycymeris* $\delta^{13}C_{shell}$ variability, multiple linear regression analyses were used to examine the combined influence of salinity, primary productivity, and the $\delta^{13}C$ composition of atmospheric CO_2 ($\delta^{13}C_{atm}$) on the *G. glycymeris* $\delta^{13}C_{shell}$ data. The $\delta^{13}C_{atm}$ record was incorporated in these analyses as an independent proxy measure of the marine Suess effect. Due to the relatively high rate of ocean-atmosphere CO_2 exchange, the surface waters of the NE Atlantic Ocean exhibits a marine Suess effect signal that is ca. 80% that of the atmospheric Suess effect (Eide et al., 2017). The multiple linear regression analyses indicate that 34% (F = 3.355; P < 0.05) and 54% (F = 7.70; P < 0.001) of the variability in the $\delta^{13}C_{high}$ and $\delta^{13}C_{low}$ series can be explained by variability in salinity, primary productivity and $\delta^{13}C_{atm}$. The increased covariance explained by the multiple linear regression models, compared to coherence found between the $\delta^{13}C_{high}$ and $\delta^{13}C_{low}$ series and individual environmental parameters, supports the hypotheses that the salinity and productivity

dynamics are driving variability in the $\delta^{13}C_{high}$ and $\delta^{13}C_{low}$ series independently.

Whilst our data do not directly evaluate the potential primary link between salinity and *G. glycymeris* $\delta^{13}C_{shell}$ variability, via carbonate anhydrase mediated $\delta^{13}C$ fractionation, these data do suggest there are likely multiple mechanisms through which environmental variability and carbon dynamics drive variability in *G. glycymeris* $\delta^{13}C_{shell}$ data. Further work is therefore required to robustly quantify the role that internal fractionation processes and external environmental carbon dynamics play in driving *G. glycymeris* $\delta^{13}C_{shell}$ variability.

3.5. Multiproxy analysis

The sensitivity of the *G. glycymeris* $\delta^{13}C_{shell}$ data to salinity variability may facilitate the application of these data in constraining uncertainties associated with $\delta^{18}O_w$ variability in $\delta^{18}O_{shell}$ derived reconstructions of past seawater temperature variability (Gillikin et al., 2006). However, the potential influence of other processes (e.g. primary productivity dynamics) on the *G. glycymeris* $\delta^{13}C_{shell}$ data, raises the potential for the stability of the relationship between salinity and $\delta^{13}C_{shell}$ to be non-stationary. To mitigate this issue we utilised the complete suite of sclerochronological records that have been developed from the Tiree Passage including the *G. glycymeris* master growth increment width sclerochronology and the co-registered $\delta^{18}O_{shell}$ series
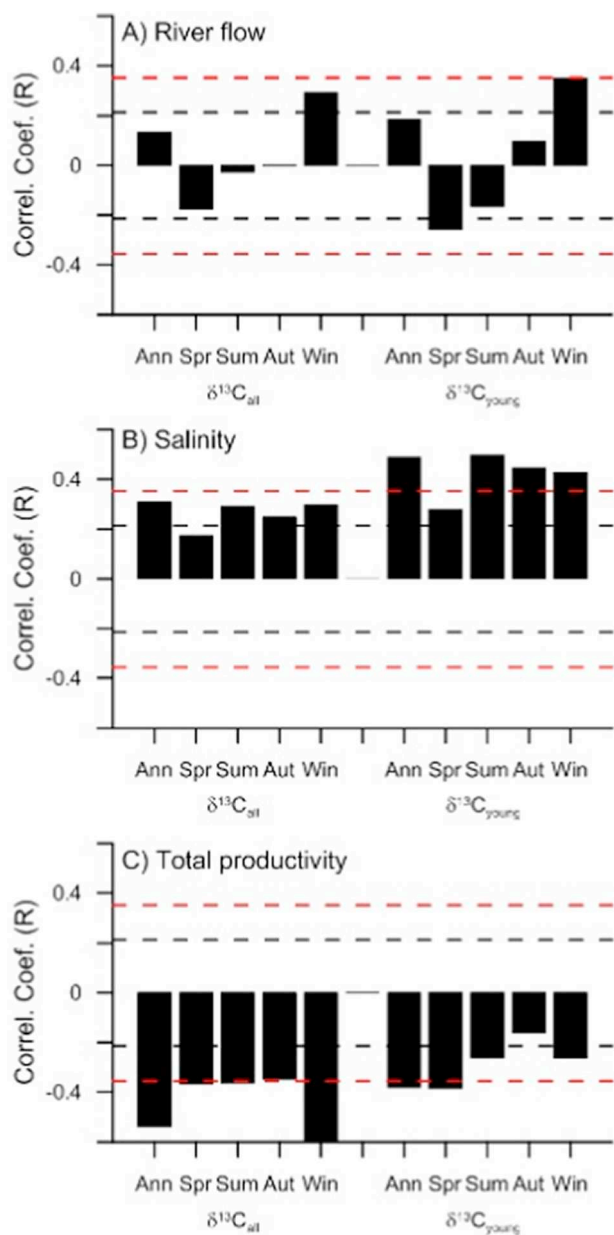
Fig. 7. Correlation coefficients calculated between the annually resolved $\delta^{1}C_{high}$ and $\delta^{13}C_{low}$ records and mean annual and seasonal A) river flow; B) SSS; and C) total productivity. The dashed black lines and dashed red lines denote the P < 0.1 and P < 0.05 significance levels respectively. Correlations calculated over the interval from 1971 to 2010 CE. Significance levels calculated using the Ebisuzaki Monte Carlo methodology. (For interpretation of the references to colour in this figure legend, the reader is referred to the web version of this article.)

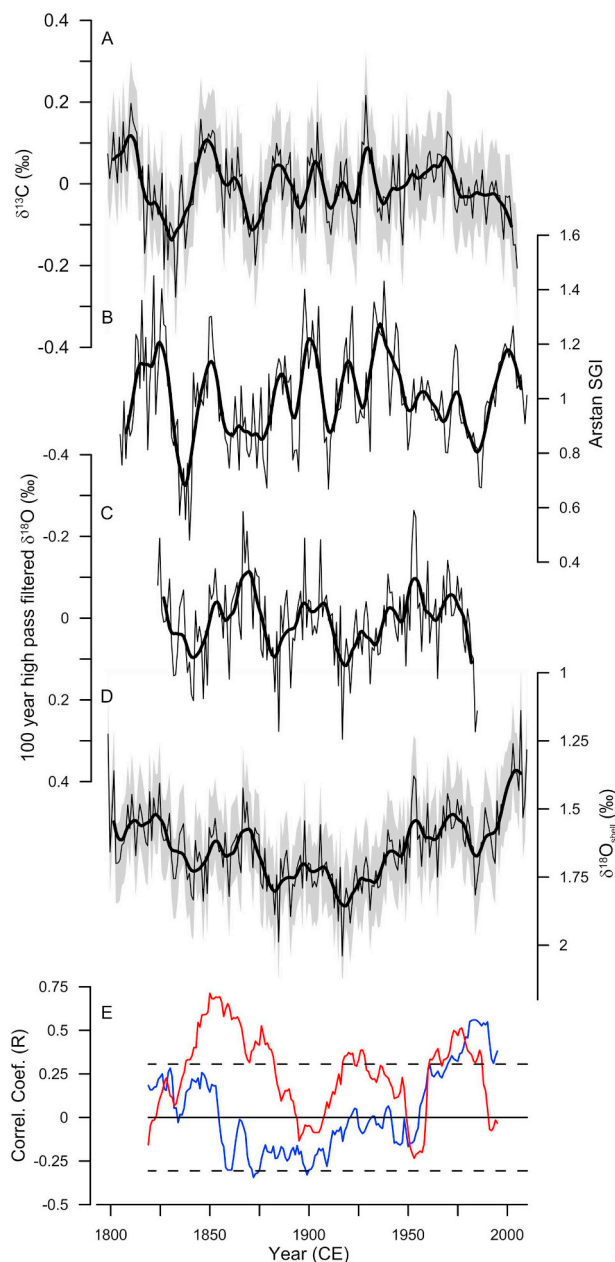**Fig. 8.** A) The annually resolved *G. glycymeris* $\delta^{13}C_{high}$ record (thin black line) plotted with a ten year first order loess low pass filter (thick black line). The record contains no long-term trends due to being constructed from linear de-trended data. The shaded grey envelope represents the RMSE of ± 0.103‰. B) The annually resolved Arstan standardised growth increment (SGI) width *G. glycymeris* chronology plotted with a 10 year first order low pass filtered data (thick black line; Reynolds et al., 2013). C) Annually resolved 100 year high pass filtered Tiree Passage $\delta^{18}O_{shell}$ data (thin black line) plotted with 10 year first order loess low pass filtered data (thick black line; Reynolds et al., 2017b). D) The annually resolved, non-detrended, Tiree Passage $\delta^{18}O_{shell}$ data (thin black line) plotted with 10 year first order loess low pass filtered data (thick black line). E) 30 year running correlations calculated between the *G. glycymeris* $\delta^{13}C$ data and *G. glycymeris* growth increment width series (red line) and between the *G. glycymeris* $\delta^{13}C_{high}$ series and $\delta^{18}O_{shell}$ record (blue line). The dashed black lines represent the P < 0.1 significance level. (For interpretation of the references to colour in this figure legend, the reader is referred to the web version of this article.)

(Reynolds et al., 2013; Reynolds et al., 2017b). The growth increment width chronology has been demonstrated to be sensitive to past seawater temperature variability, biological productivity (both primary productivity and zooplankton abundance) and seawater salinity variability (Reynolds et al., 2013; Reynolds et al., 2017b). Previous analyses suggest that, over the instrumental period (1954–2010), the *G. glycymeris* $\delta^{18}O_{shell}$ series is dominated by seawater temperature variability (Reynolds et al., 2017b). However, given that $\delta^{18}O_{arg}$, and therefore $\delta^{18}O_{shell}$, variability is associated with both seawater temperature and $\delta^{18}O_w$ variability, it is likely that during periods when salinity variability is greater than over the current observational period $\delta^{18}O_w$ variability likely played a greater role in shaping the $\delta^{18}O_{shell}$

variability.

Utilising the *G. glycymeris* $\delta^{13}C_{shell}$, growth increment width series and $\delta^{18}O_{shell}$ series, whilst potentially useful, also present significant

challenges. Whilst all three series are annually resolved and absolutely dated the presence of ontogenetic trends in both the raw growth increment and $\delta^{13}C_{shell}$ series necessitates the long-term $\delta^{13}C_{shell}$ and growth increment width series being constructed from detrended data. Thus, both the $\delta^{13}C_{high}$ and growth increment width series lack long-term variability. Whilst utilising the $\delta^{13}C_{low}$ series can mitigate this issue, this series is discontinuous over the duration of the time period covered by the $\delta^{18}O_{shell}$ record and can thus only provide snapshots of the uncertainty associated with lower frequency $\delta^{18}O_w$ variability.

Despite the complications, comparison between the co-registered *G. glycymeris* sclerochronologically derived records ($\delta^{13}C_{high}$ and $\delta^{13}C_{low}$, $\delta^{18}O_{shell}$ and the growth increment width series) highlights that the *G. glycymeris* $\delta^{13}C_{high}$ record exhibits significant positive 30 year running correlations (P < 0.1) with the *G. glycymeris* growth increment width series (Fig. 8). However, there are two notable intervals (1883–1918 and 1940–1960 CE) that contain no significant correlation. A peak correlation of $R = 0.7$ occurs between the interval of 1840–1860 CE. The running correlations calculated between the *G. glycymeris* $\delta^{13}C_{high}$ and high pass filtered $\delta^{18}O_{shell}$ records contain no consistent significant correlation over the interval between 1820 and 1970 CE, although the correlations are significant (P < 0.1) in the years 1872, 1873 and 1900 CE. Between 1972 and 1995 CE the $\delta^{13}C_{high}$ and $\delta^{18}O_{shell}$ records significantly correlate (mean $R = 0.45$, P < 0.1).

Given that both the *G. glycymeris* $\delta^{13}C_{high}$ data and corresponding growth increment width series both independently positively correlate with salinity in the Sea of the Hebrides, the significant positive correlations between the $\delta^{13}C_{high}$ and growth increment width series suggest that the $\delta^{13}C_{high}$ record is being primarily driven by salinity variability. Whilst both the $\delta^{13}C_{high}$ and growth increment width series both also correlate with primary production, if primary production were to be the dominant driver of the $\delta^{13}C_{high}$ record, one would assume the correlations between the $\delta^{13}C_{high}$ and growth increment width series should be negative. This is because the $\delta^{13}C_{high}$ data negatively correlate with primary production, whilst the growth increment series positively correlate with primary production (Reynolds et al., 2017b). However, whilst the running correlations calculated between the $\delta^{13}C_{high}$ record and the growth increment width series are generally significant, there are two notable intervals where the correlations are not significant. This suggests that during these intervals it is likely that salinity variability is playing less of a role in driving the $\delta^{13}C_{shell}$ variability or being masked by other processes (e.g. primary production, shifts in background $\delta^{13}C_{DIC}$).

The examination of the running correlation analyses indicates that, except during two periods (1872–3 and 1900 CE), the $\delta^{13}C_{high}$ data and high pass filtered $\delta^{18}O_{shell}$ records are not significantly correlated over the interval from 1820 to 1972 CE. The lack of coherence between the $\delta^{13}C_{high}$ and $\delta^{18}O_{shell}$ variability over this interval suggests that salinity variability is likely not having a significant impact on the $\delta^{18}O_{shell}$ variability. However, over the interval from 1973 to 1995 the $\delta^{13}C_{high}$ data and $\delta^{18}O_{shell}$ record do significantly correlate (mean R = 0.45 P < 0.1). The significant positive correlation suggests that, over this recent interval, salinity variability would likely lead to increased uncertainties in the resulting $\delta^{18}O_{shell}$ based temperature reconstruction. However, integrating the $\delta^{13}C_{high}$ and $\delta^{13}C_{low}$ data and instrumental salinity data, as proxies for $\delta^{18}O_w$, with the $\delta^{18}O_{shell}$ to quantify these uncertainties yields reconstructed seawater temperatures that are highly coherent ($R = 0.98$ to 0.99; Fig. 9). These data suggest that mean annual salinity varied between 34.6 and 35 units over the reconstructed period, which would equate to a maximum shift of 0.05‰ in $\delta^{18}O_w$, and a shift in reconstructed seawater temperatures of 0.22 °C (assuming a 4.3 °C shift in temperature per 1‰ shift in $\delta^{18}O$). This amplitude of $\delta^{18}O_w$ variability therefore only drives a relatively small shift in the corresponding reconstructed seawater temperatures. The total 0.22 °C shift due to salinity is relatively small in amplitude relative to the range in reconstructed temperatures (ca. 2.9 °C) as well as the mean shift in temperature from year to year (0.6 °C).
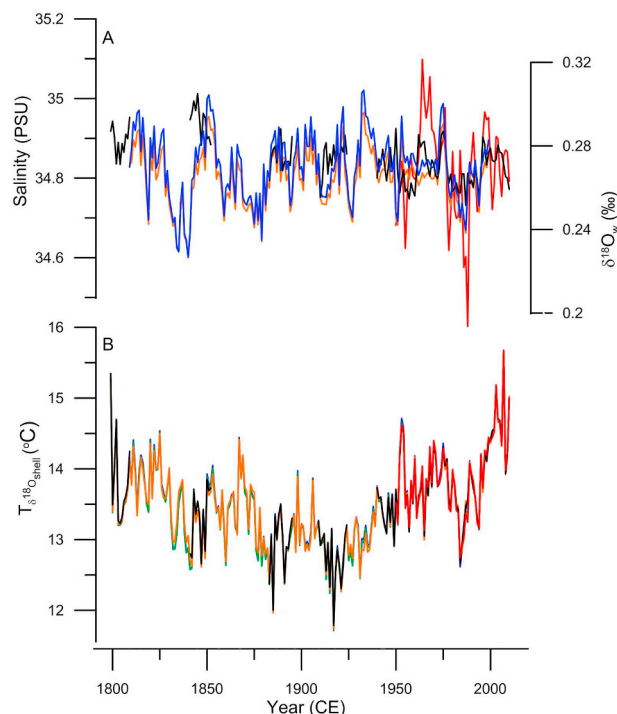

Fig. 9. A) The $\delta^{13}C_{low}$ and $\delta^{13}C_{high}$ data (black and orange lines respectively) plotted as reconstructed SSS and $\delta^{18}O_w$. The blue line shows reconstructed salinity and corresponding $\delta^{18}O_w$ values derived using the PC1 of the Arstan growth increment series, the $\delta^{13C high}$ and 45 year high pass filtered $\delta^{18}O_{shell}$ record. The red line shows instrumental SSS data and corresponding $\delta^{18}O_w$ values. B) Reconstructed SSTs derived using the $\delta^{13}C_{low}$, $\delta^{13}C_{high}$ PC1, instrumental SSS derived $\delta^{18}O_w$ values (black, orange, blue and red lines respectively) and using a constant $\delta^{18}O_w$ value based on the mean of the instrumental data (green line). (For interpretation of the references to colour in this figure legend, the reader is referred to the web version of this article.)

4. Conclusions

This study demonstrates that $\delta^{13}C_{shell}$ data derived from *G. glycymeris* growth increments older than 20 years of age contain significant ontogenetic trends. These trends must therefore be removed prior to the application of these data in reconstructing environmental variability. By utilising $\delta^{13}C_{shell}$ data derived from growth increments < 20 years of age, or by applying simple detrending techniques, it is possible to use *G. glycymeris* $\delta^{13}C_{shell}$ data to evaluate past environmental variability. These analyses demonstrate that variability in the *G. glycymeris* $\delta^{13}C_{shell}$ data covaries with salinity and primary productivity in the Sea of the Hebrides and adjacent waters. The integrated analysis of the $\delta^{13}C_{shell}$ data with co-registered $\delta^{18}O_{shell}$ data and the *G. glycymeris* growth increment width series facilitates the identification of portions of the δ13C_shell data that are dominated by salinity variability and ultimately when periods of the $\delta^{18}O_{shell}$ record are dominated by salinity variability. These data therefore can ultimately be used to further constrain the uncertainties past environmental variability and the impacts on marine carbon dynamics.

Data availability

The Continuous Plankton recorder data are available at https://www.sahfos.ac.uk/DOI:10.7487/2017.216.1.1072. The Carbon isotope data presented in this manuscript are available via the NCDC webpage https://www.ncdc.noaa.gov/paleo-search/study/22621.

Appendix A. Supplementary data

Supplementary data to this article can be found online at https://doi.org/10.1016/j.palaeo.2019.03.005.

References

Beirne, E.C., Wanamaker Jr., A.D., Feindel, S.C., 2012. Experimental validation of environmental controls on the delta C-13 of *Arctica islandica* (ocean quahog) shell carbonate. Geochim. Cosmochim. Acta 84, 395–409.

Brocas, W.M., Reynolds, D.J., Butler, P.G., Richardson, C.A., Scourse, J.D., Ridgway, I.D., Ramsay, K., 2013. The dog cockle, *Glycymeris glycymeris* (L.), a new annually-resolved sclerochronological archive for the Irish Sea. Palaeogeogr. Palaeoclimatol. Palaeoecol. 373, 133–140.

Butler, P.G., Scourse, J.D., Richardson, C.A., Wanamaker Jr., A.D., Bryant, C.L., Bennell, J.D., 2009. Continuous marine radiocarbon reservoir calibration and the C-13 Suess effect in the Irish Sea: results from the first multi-centennial shell-based marine master chronology. Earth Planet. Sci. Lett. 279, 230–241.

Butler, P.G., Richardson, C.A., Scourse, J.D., Wanamaker, A.D., Shammon, T.M., Bennell, J.D., 2010. Marine climate in the Irish Sea: analysis of a 489-year marine master chronology derived from growth increments in the shell of the clam *Arctica islandica*. Quat. Sci. Rev. 29, 1614–1632.

Cage, A.G., Austin, W.E.N., 2010. Marine climate variability during the last millennium: the Loch Sunart record, Scotland, UK. Quat. Sci. Rev. 29, 1633–1647.

Cage, A.G., Heinemeier, J., Austin, W.E.N., 2006. Marine radiocarbon reservoir ages in Scottish coastal and fjordic waters. Radiocarbon 48, 31–43.

Chappell, J., Shackleton, N.J., 1986. Oxygen isotopes and sea-level. Nature 324, 137–140.

Chappell, J., Omura, A., Esat, T., Mcculloch, M., Pandolfi, J., Ota, Y., Pillans, B., 1996. Reconciliation of late Quaternary sea levels derived from coral terraces at Huon Peninsula with deep sea oxygen isotope records. Earth Planet. Sci. Lett. 141, 227–236.

Chauvaud, L., Thebault, J., Clavier, J., Lorrain, A., Strand, O., 2011. What's hiding behind ontogenetic delta C-13 variations in mollusk shells? New insights from the great scallop (*Pecten maximus*). Estuar. Coasts 34, 211–220.

Cook, E.R., Briffa, K.R., Meko, D.M., Graybill, D.A., Funkhouser, G., 1995. The 'segment length curse' in long tree-ring chronology development for palaeoclimatic studies. The Holocene 5.

Eide, M., Olsen, A., Ninnemann, U.S., Eldevik, T., 2017. A global estimate of the full oceanic C-13 Suess effect since the preindustrial. Glob. Biogeochem. Cycles 31, 492–514.

Elderfield, H., Ganssen, G., 2000. Past temperature and delta O-18 of surface ocean waters inferred from foraminiferal Mg/Ca ratios. Nature 405, 442–445.

Esper, J., Cook, E.R., Schweingruber, F.H., 2002. Low-frequency signals in long tree-ring chronologies for reconstructing past temperature variability. Science 295, 2250–2253.

Fairbanks, R.G., Matthews, R.K., 1978. Marine oxygen isotope record in Pleistocene coral, Barbados, West-Indies. Quat. Res. 10, 181–196.

Featherstone, A. M., Butler, P. G., Peharda, M., Chauvaud, L. & Thebault, J. 2017. Influence of riverine input on the growth of *Glycymeris glycymeris* in the Bay of Brest, North-West France. Plos One, 12.

Francey, R.J., Allison, C.E., Etheridge, D.M., Trudinger, C.M., Enting, I.G., Leuenberger, M., Langenfelds, R.L., Michel, E., Steele, L.P., 1999. A 1000-year high precision record of delta C-13 in atmospheric CO2. Tellus Ser. B Chem. Phys. Meteorol. 51, 170–193.

Freitas, P., Clarke, L. J., Kennedy, H., Richardson, C. & Abrantes, F. 2005. Mg/Ca,Sr/Ca, and stable-isotope (delta O-18 and delta C-13) ratio profiles from the fan mussel *Pinna nobilis*: Seasonal records and temperature relationships. Geochem. Geophys. Geosyst., 6.

Freitas, P.S., Clarke, L.J., Kennedy, H.A., Richardson, C.A., 2008. Inter- and intra-specimen variability masks reliable temperature control on shell Mg/Ca ratios in laboratory- and field-cultured *Mytilus edulis* and *Pecten maximus* (bivalvia). Biogeosciences 5, 1245–1258.

Freitas, P.S., Clarke, L.J., Kennedy, H., Richardson, C.A., 2012. The potential of combined Mg/Ca and δ18O measurements within the shell of the bivalve *Pecten maximus* to estimate seawater δ18O composition. Chem. Geol. 291, 286–293.

Gagen, M., Mccarroll, D., Robertson, I., Loader, N.J., Jalkanen, R., 2008. Do tree ring delta C-13 series from *Pinus sylvestris* in northern Fennoscandia contain long-term non-climatic trends? Chem. Geol. 252, 42–51.

Galbraith, E.D., Kwon, E.Y., Bianchi, D., Hain, M.P., Sarmiento, J.L., 2015. The impact of atmospheric pCO(2) on carbon isotope ratios of the atmosphere and ocean. Glob. Biogeochem. Cycles 29, 307–324.

Gilles, R. 1972. Osmoregulation in 3 molluscs - *acanthochitona-discrepans* (brown), *Glycymeris glycymeris* (l) and *Mytilus-edulis* (l). *Biological Bulletin,* 142, 25-&.

Gillikin, D.P., De Ridder, F., Ulens, H., Elskens, M., Keppens, E., Baeyens, W., Dehairs, F.,

2005. Assessing the reproducibility and reliability of estuarine bivalve shells (*Saxidomus giganteus*) for sea surface temperature reconstruction: Implications for paleoclimate studies. Palaeogeogr. Palaeoclimatol. Palaeoecol. 228, 70–85.

Gillikin, D.P., Lorrain, A., Bouillon, S., Willenz, P., Dehairs, F., 2006. Stable carbon isotopic composition of *Mytilus edulis* shells: relation to metabolism, salinity, delta C-13(DIC) and phytoplankton. Org. Geochem. 37, 1371–1382.

Gillikin, D.P., Lorrain, A., Meng, L., Dehairs, F., 2007. A large metabolic carbon contribution to the delta C-13 record in marine aragonitic bivalve shells. Geochim. Cosmochim. Acta 71, 2936–2946.

Good, S.A., Martin, M.J., Rayner, N.A., 2013. EN4: Quality controlled ocean temperature and salinity profiles and monthly objective analyses with uncertainty estimates. J. Geophys. Res. Oceans 118, 6704–6716.

Goodwin, D.H., Gillikin, D.P., Roopnarine, P.D., 2013. Preliminary evaluation of potential stable isotope and trace element productivity proxies in the oyster *Crassostrea gigas*. Palaeogeogr. Palaeoclimatol. Palaeoecol. 373, 88–97.

Grossman, E., Ku, T., 1986. Oxygen and carbon isotope fractionation in biogenic aragonite: Temperature effects. Chem. Geol. 59, 59–74. https://doi.org/10.1016/0168-9622(86)90057-6.

Hayward, P.J., Ryland, J.S., 1995. Handbook of the Marine Fauna of North-West Europe. Oxford University Press.

Henry, R.P., Saintsing, D.G., 1983. Carbonic-anhydrase activity and ion regulation in 3 species of osmoregulating bivalve mollusks. Physiol. Zool. 56, 274–280.

Inall, M., Gillibrand, P., Griffiths, C., Macdougal, N., Blackwell, K., 2009. On the oceanographic variability of the North-West European Shelf to the West of Scotland. J. Mar. Syst. 77, 210–226.

Jickells, T.D., 1998. Nutrient biogeochemistry of the coastal zone. Science 281, 217–222.

Keeling, C.D., Guenther, P., 1994. Shore based carbon analysis: duplicate carbon measurements made by the Carbon Dioxide Research Group — Scripps Institution of Oceanography, University of California, San Diego. http://cdiac.esd.ornl.gov/ftp/oceans/keeling.data/. Carbon Dioxide Information Analysis Center, Oak Ridge National Laboratory, US Department of Energy, Oak Ridge, Tennessee.

Keller, N., Del Piero, D., Longinelli, A., 2002. Isotopic composition, growth rates and biological behaviour of *Chamelea gallina* and *Callista chione* from the Gulf of Trieste (Italy). Mar. Biol. 140, 9–15.

Kennedy, H., Richardson, C.A., Duarte, C.M., Kennedy, D.P., 2001. Oxygen and carbon stable isotopic profiles of the fan mussel, *Pinna nobilis*, and reconstruction of sea surface temperatures in the Mediterranean. Mar. Biol. 139, 1115–1124.

Klein, R.T., Lohmann, K.C., Thayer, C.W., 1996. SrCa and 13C12C ratios in skeletal calcite of *Mytilus trossulus*: Covariation with metabolic rate, salinity, and carbon isotopic composition of seawater. Geochim. Cosmochim. Acta 60 (21), 4207–4221.

Krantz, D.E., Williams, D.F., Jones, D.S., 1987. Ecological and paleoenvironmental information using stable isotope profiles from living and fossil mollusks. Palaeogeogr. Palaeoclimatol. Palaeoecol. 58, 249–266.

Lorens, R.B., Bender, M.L., 1980. The impact of solution chemistry on *Mytilus edulis* calcite and aragonite. Geochim. Cosmochim. Acta 44, 1265–1278.

Lorrain, A., Paulet, Y.M., Chauvaud, L., Dunbar, R., Mucciarone, D., Fontugne, M., 2004. Delta C-13 variation in scallop shells: increasing metabolic carbon contribution with body size? Geochim. Cosmochim. Acta 68, 3509–3519.

Lorrain, A., Gillikin, D.P., Paulet, Y.M., Chauvaud, L., Le Mercier, A., Navez, J., André, L., 2005. Strong kinetic effects on Sr/Ca ratios in the calcitic bivalve *Pecten maximus*. Geology 33 (12), 965–968.

Lynch-Stieglitz, J., Stocker, T.F., Broecker, W.S., Fairbanks, R.G., 1995. The influence of air-sea exchange on the isotopic composition of oceanic carbon - observations and modeling. Glob. Biogeochem. Cycles 9, 653–665.

Marsh, R., Haigh, I. D., Cunningham, S. A., Inall, M. E., Porter, M. & Moat, B. I. 2017. Large-scale forcing of the European Slope Current and associated inflows to the North Sea. Ocean Science, 13.

McConnaughey, T.A., Gillikin, D.P., 2008. Carbon isotopes in mollusk shell carbonates. Geo-Mar. Lett. 28 (5–6), 287–299.

McConnaughey, T.A., Burdett, J., Whelan, J.F., Paull, C.K., 1997. Carbon isotopes in biological carbonates: respiration and photosynthesis. Geochim. Cosmochim. Acta 61 (3), 611–622.

Mook, W.G., Tan, F.C., 1991. Stable carbon isotopes in rivers and estuaries. In: Kempe, S., Richey, J.E. (Eds.), Degens, E.T. Biogeochemistry of Major World Rivers, John Wiley and Sons Ltd, pp. 245–264.

Olsen, A., Ninnemann, U., 2010. Large delta C-13 gradients in the preindustrial north atlantic revealed. Science 330, 658–659.

Ramsay, K., Kaiser, M.J., Richardson, C.A., Veale, L.O., Brand, A.R., 2000. Can shell scars on dog cockles (*Glycymeris glycymeris* L.) be used as an indicator of fishing disturbance? J. Sea Res. 43, 167–176.

Ramsay, C.B., 2009. Bayesian analysis of radiocarbon dates. Radiocarbon 51, 337–360.

Rayner, N.A., Parker, D.E., Horton, E.B., Folland, C.K., Alexander, L.V., Rowell, D.P., Kent, E.C., Kaplan, A., 2003. Global analyses of sea surface temperature, sea ice, and night marine air temperature since the late nineteenth century. J. Geophys. Res.-Atmos. 108.

Reimer, P.J., Bard, E., Bayliss, A., Beck, J.W., Blackwell, P.G., Ramsey, C.B., Buck, C.E., Cheng, H., Edwards, R.L., Friedrich, M., Grootes, P.M., Guilderson, T.P., Haflidason, H., Hajdas, I., Hatte, C., Heaton, T.J., Hoffmann, D.L., Hogg, A.G., Hughen, K.A., Kaiser, K.F., Kromer, B., Manning, S.W., Niu, M., Reimer, R.W., Richards, D.A., Scott, E.M., Southon, J.R., Staff, R.A., Turney, C.S.M., Van Der Plicht, J., 2013. Intcal13 and marine13 radiocarbon age calibration curves 0-50,000 years Cal BP. Radiocarbon 55, 1869–1887.

Reynolds, D.J., 2011. Establishing Multi-Bivalve Species Sclerochronology. Bangor University.

Reynolds, D.J., Butler, P.G., Williams, S.M., Scourse, J.D., Richardson, C.A., Wanamaker, A.D., Austin, W.E.N., Cage, A.G., Sayer, M.D.J., 2013. A multiproxy reconstruction of

Hebridean (NW Scotland) spring sea surface temperatures between AD 1805 and 2010. Palaeogeogr. Palaeoclimatol. Palaeoecol. 386, 275–285.

Reynolds, D. J., Scourse, J. D., Halloran, P. R., Nederbragt, A. J., Wanamaker, A. D., Butler, P. G., Richardson, C. A., Heinemeier, J., Eiriksson, J., Knudsen, K. L. & Hall, I. R. 2016. Annually resolved North Atlantic marine climate over the last millennium. Nature Communications, 7.

Reynolds, D.J., Hall, I.R., Scourse, J.D., Richardson, C.A., Wanamaker, A.D., Butler, P.G., 2017a. Biological and climate controls on north Atlantic marine carbon dynamics over the last millennium: insights from an absolutely dated shell-based record from the North Icelandic Shelf. Glob. Biogeochem. Cycles 31, 1718–1735.

Reynolds, D. J., Hall, I. R., Slater, S., Scourse, J. D., Halloran, P. R. & Sayer, M. D. J. 2017b. Reconstructing past seasonal to multi-centennial scale variability in the NE Atlantic Ocean using the long-lived marine bivalve mollusc *Glycymeris glycymeris*. Paleocanography.

Richardson, C.A., 2001. Molluscs as archives of environmental change. Oceanogr. Mar. Biol. 39 (39), 103–164.

Royer, C., Thebault, J., Chauvaud, L., Olivier, F., 2013. Structural analysis and paleoenvironmental potential of dog cockle shells (*Glycymeris glycymeris*) in Brittany, Northwest France. Palaeogeogr. Palaeoclimatol. Palaeoecol. 373, 123–132.

Schöne, B.R., Fiebig, J., Pfeiffer, M., Gless, R., Hickson, J., Johnson, A.L.A., Dreyer, W., Oschmann, W., 2005. Climate records from a bivalved Methuselah (*Arctica islandica*, Mollusca; Iceland). Palaeogeogr. Palaeoclimatol. Palaeoecol. 228, 130–148.

Schöne, B.R., Wanamaker, A.D., Fiebig, J., Thébault, J., Kreutz, K., 2011. Annually resolved δ13Cshell chronologies of long-lived bivalve mollusks (*Arctica islandica*) reveal oceanic carbon dynamics in the temperate North Atlantic during recent centuries. Palaeogeogr. Palaeoclimatol. Palaeoecol. 302, 31–42.

Shackleton, N.J., Backman, J., Zimmerman, H., Kent, D.V., Hall, M.A., Roberts, D.G., Schnitker, D., Baldauf, J.G., Desprairies, A., Homrighausen, R., Huddlestun, P., Keene, J.B., Kaltenback, A.J., Krumsiek, K.A.O., Morton, A.C., Murray, J.W., Westbergsmith, J., 1984. Oxygen isotope calibration of the onset of ice-rafting and

history of glaciation in the North-Atlantic region. Nature 307, 620–623.

Suess, H.E., 1953. Natural radiocarbon and the rate of exchange of carbon dioxide between the atmosphere and the sea. In: Aldrich, W. (Ed.), Nuclear Processes in Geologic Settings. University of Chicago Press, Chicago.

Tanaka, N., Monaghan, M.C., Rye, D.M., 1986. Contribution of metabolic carbon to mollusc and barnacle shell carbonate. Nature 320 (6062), 520.

Trouet, V., Van Oldenborgh, G.J., 2013. Climate explorer: a web-based research tool for high-resolution paleoclimatology. Tree-Ring Res. 69, 3–13.

Urey, H.C., 1948. Oxygen isotopes in nature and in the laboratory. Science 108, 489–496.

Vander Putten, E., Dehairs, F., Keppens, E., Baeyens, W., 2000. High resolution distribution of trace elements in the calcite shell layer of modern *Mytilus edulis*: environmental and biological controls. Geochim. Cosmochim. Acta 64, 997–1011.

Wanamaker, A.D., Kreutz, K.J., Schoene, B.R., Pettigrew, N., Borns, H.W., Introne, D.S., Belknap, D., Maasch, K.A., Feindel, S., 2008a. Coupled North Atlantic slope water forcing on Gulf of Maine temperatures over the past millennium. Clim. Dyn. 31, 183–194.

Wanamaker, A.D., Kreutz, K.J., Wilson, T., Borns, H.W., Introne, D.S., Feindel, S., 2008b. Experimentally determined Mg/Ca and Sr/Ca ratios in juvenile bivalve calcite for *Mytilus edulis*: implications for paleotemperature reconstructions. Geo-Mar. Lett. 28, 359–368.

Wanamaker, A.D., Kreutz, K.J., Schone, B.R., Maasch, K.A., Pershing, A.J., Borns, H.W., Introne, D., Feindel, S., 2009. A late Holocene paleo-productivity record in the western Gulf of Maine, USA, inferred from growth histories of the long-lived ocean quahog (*Arctica islandica*). Int. J. Earth Sci. 98, 19–29.

Wanamaker Jr., A.D., Kreutz, K.J., Schoene, B.R., Introne, D.S., 2011. Gulf of Maine shells reveal changes in seawater temperature seasonality during the medieval climate anomaly and the little ice age. Palaeogeogr. Palaeoclimatol. Palaeoecol. 302, 43–51.

Wigley, T.M.L., Jones, P.D., Briffa, K.R., 1987. Cross-Dating Methods in Dendrochronology. J. Archaeol. Sci. 14, 51–64.